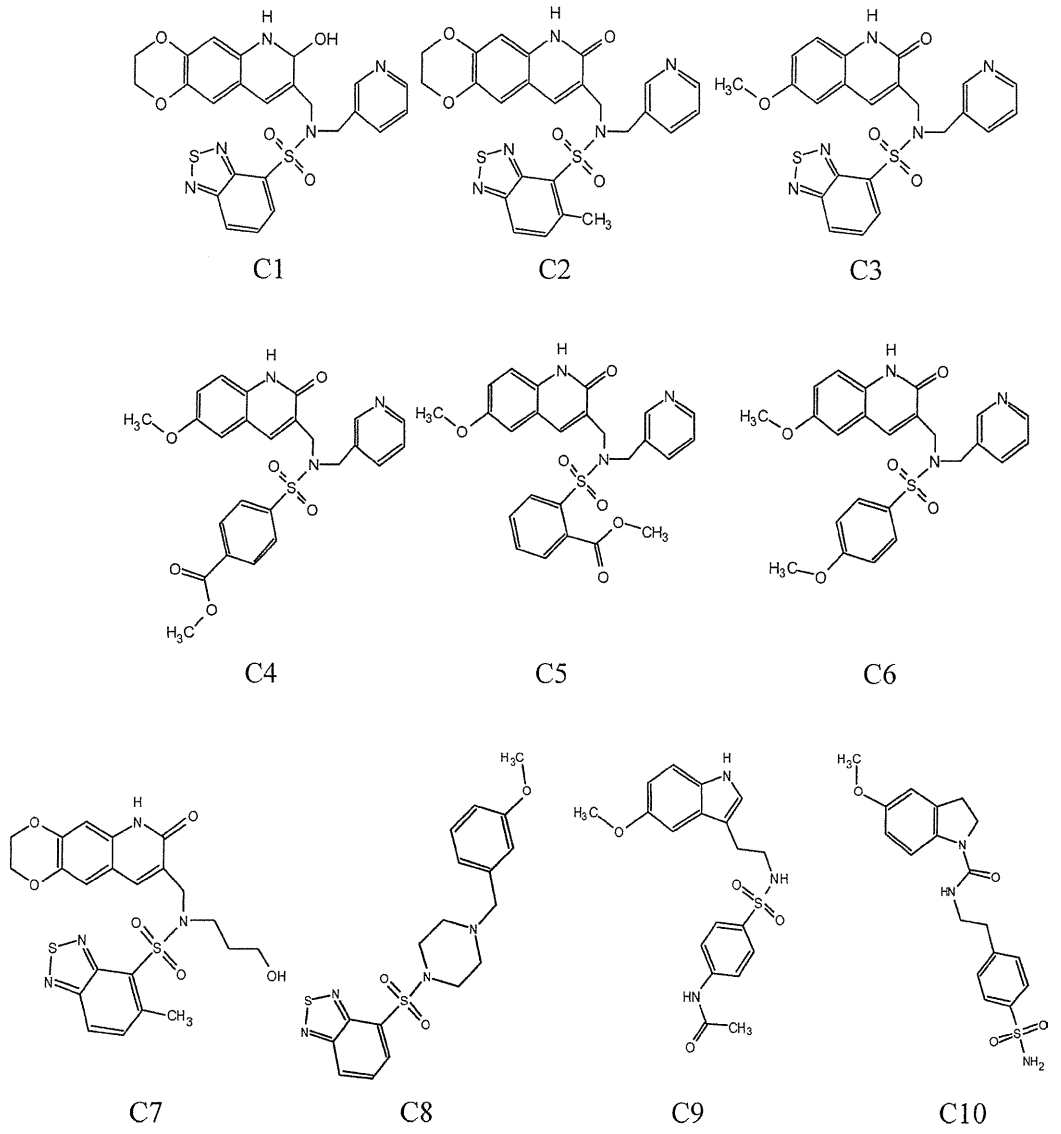

FIG 2 Chemical structures of compounds. C1 and C2 were identified by *in silico* screening. C3 to C10 were searched by PubChem (http://pubchem.ncbi.nlm.nih.gov/).

tured at a ratio of 1:5 with fresh medium containing appropriate concentrations of the compounds and further incubated for 3 days. The cytotoxicity of the compounds was evaluated in parallel with their antiviral activity, which was based on the reduction of the viability of non-TNF-α-treated OM-10.1 and U1 cells or mock-infected CEM cells, MOLT-4 cells, and PBMCs by the 3-(4,5-dimethylthiazol-2-yl)-2,5-diphenyltetrazolium bromide (MTT) method, as previously described (30). The 50% effective concentrations (EC_{50}) and 50% cytotoxic concentrations (CC_{50}s) were determined by the median-effect method (31).

Reporter assays. W-3 and KM-3 cells (1×10^5 cells/ml) were either treated with 10 ng/ml of TNF-α (Roche Diagnostics) or transfected with 0.2 μg of an HIV-1 Tat expression plasmid containing the second exon under the control of the simian virus 40 promoter (modification of pSV2tat72) with a Gene Pulser II (300 V and 1,000 μF; Bio-Rad Laboratories, Hercules, CA) (25). The cells were cultured in the presence of various concentrations of the compounds. After incubation for 24 h at 37°C, the culture supernatants were collected, incubated for 30 min at 65°C to inactivate the alkaline phosphatase activity of fetal bovine serum in culture medium, and examined for their SEAP levels using the GreatEscape SEAP detection kit (Clontech, Palo Alto, CA). The chemiluminescence intensity was measured with a TriStar Multimode Microplate Reader LB 941 (Berthold Technologies, Bad Wildbad, Germany). At the same time, the viable cell number was determined by a dye method using a water-soluble tetrazolium, Tetracolor One (Seikagaku Corporation, Tokyo, Japan).

Western blot analysis. W-3 cells (1×10^5 cells/ml) were transfected with 0.2 μg of the Tat expression plasmid and cultured in the presence of various concentrations of the compounds. After incubation for 2 days at 37°C, the cells were washed and lysed with an assay buffer for immunoprecipitation (Nacalai Tesque, Kyoto, Japan). The cell lysates were separated by sodium dodecyl sulfate polyacrylamide gel electrophoresis (SDS-PAGE) with a 10% gel, and the separated proteins were electrophoretically transferred to a polyvinylidene difluoride membrane (Immobilon-P; Millipore, Billerica, MA) using a semidry transfer apparatus (Bio-Rad Laboratories). The membrane was incubated with anti-phosphorylated RNAPII (Ser2) (Novus Biologicals Inc., Littleton, CO), anti-RNAPII (Novus

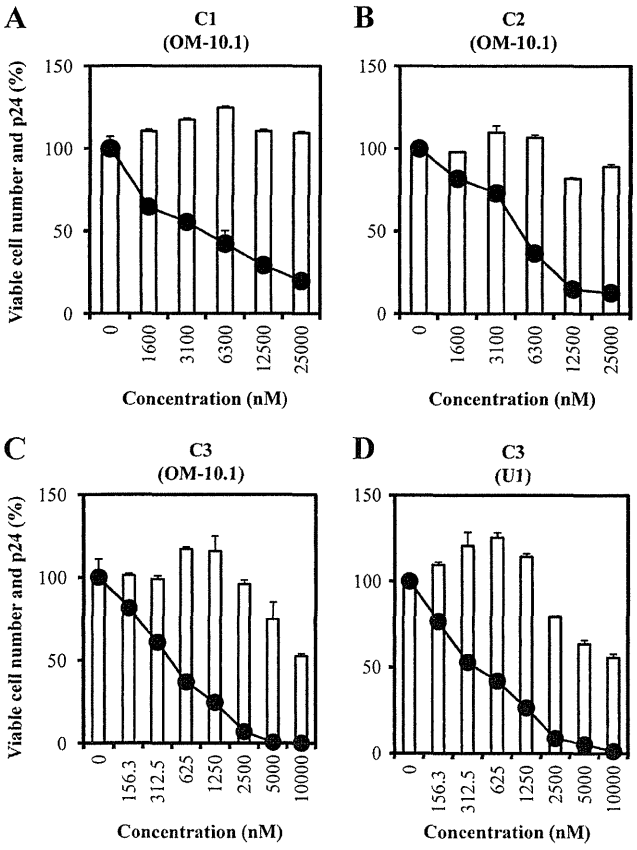

FIG 3 Anti-HIV-1 activity of C1 to C3 in chronically infected cells. OM-10.1 (A to C) and U1 (D) cells were incubated in the presence of various concentrations of the test compounds. After incubation for 24 h, the cells were stimulated with TNF-α (0.1 ng/ml) for 72 h. The p24 levels in the culture supernatants (circles with line) and cell viability (bars) were determined by ELISA and the MTT method, respectively. Data are expressed as the percentage of controls (p24 level and viable cell number in the absence of compounds). All experiments were carried out in duplicate, and mean values and standard errors are shown.

Biologicals), and anti-glyceraldehyde-3-phosphate dehydrogenase (anti-GAPDH; Santa Cruz Biotechnology, Santa Cruz, CA) antibodies. After being washed three times with phosphate-buffered saline containing Tween 20 (0.1%) (PBS-T), the membrane was further incubated with a horseradish peroxidase (HRP)-conjugated anti-rabbit IgG antibody (Cell Signaling Technology, Danvers, MA) or HRP-conjugated anti-mouse IgG1 antibody (Jackson ImmunoResearch Laboratories, West Grove, PA). The membrane was washed three times with PBS-T and analyzed for chemiluminescence by Chmi-Lumi One (Nacalai Tesque).

Immunoprecipitation. Dynabeads protein G (Invitrogen Dynal, Oslo, Norway) immobilized with an anti-CycT1 antibody (Santa Cruz Biotechnology) or goat IgG (Jackson ImmunoResearch, West Grove, PA) was incubated with CEM cell lysate for 1 h at 4°C. Tat (Immuno Diagnostics, Woburn, MA) was reconstituted in binding buffer (50 mM Tris-HCl [pH 7.5] and 0.5% NP-40) containing 120 mM NaCl, 400 μM $ZnSO_4$, and 1 mM dithiothreitol (DTT) for 1 h at room temperature. The beads were washed with binding buffer containing 120 mM NaCl and incubated in the presence of various concentrations of C3 and the reconstituted Tat in binding buffer containing 120 mM NaCl and 10% bovine serum albumin (BSA). After incubation for 2 h at 4°C, the beads were washed three times with binding buffer containing 500 mM NaCl at room temperature. The beads were boiled in SDS sample buffer, and the supernatant was subjected to SDS-PAGE with a 15% gel. Western blot analysis was performed with anti-CycT1 (Santa Cruz Biotechnology), anti-CDK9 (Santa Cruz Biotechnology), and anti-Tat (Immuno Diagnostics) antibodies.

RESULTS

***In silico* screening of compounds.** To identify small-molecule inhibitors of HIV-1 transcription, we decided to perform *in silico* screening of compounds targeting the TRM of CycT1, which interacts with Tat and TAR RNA. To this end, we constructed a homology model of human CycT1 based on the structure of equine CycT1/EIAV Tat/TAR RNA complex. When the target sites for *in silico* screening were searched in the constructed human CycT1 model using MOE software, one site that included the TRM and might interact with small molecules was found. This site was composed of 21 amino acids of CycT1, Q162, L163, R165, A166, S167, D169, L170, Q172, F176, V199, C200, L203, A204, K206, L234, L237, T238, N250, K253, W258, and R259 (Fig. 1). Among these, N250 and R259 interact with Tat, and W258 binds to TAR RNA (13). Q172 and F176 do not belong to the TRM, but these amino acids interact with Tat in the crystallographic structure of the human CycT1/Tat complex (15). We conducted *in silico* screening of compounds for this site, and the obtained data were sorted by docking energy scores calculated with MOE software. Then, 124 compounds with high docking energy scores were chosen and examined for their inhibitory effect on HIV-1 replication in TNF-α-stimulated OM-10.1 cells. Among them, two structurally related compounds (C1 and C2) (Fig. 2) proved inhibitory to HIV-1 replication in a dose-dependent manner (Fig. 3A and B). The 50% effective concentrations (EC_{50}s) of C1 and C2 were 4.2 and 4.8 μM, respectively. Neither compound showed any cytotoxicity at concentrations up to 25 μM.

Anti-HIV-1 activity *in vitro*. To find more potent compounds, derivatives of C1 and C2 were searched using PubChem (http://pubchem.ncbi.nlm.nih.gov/), and 8 compounds (C3 to C10) were identified (Fig. 2). While C4 to C10 did not inhibit HIV-1 replication in TNF-α-stimulated OM-10.1 cells (data not shown), C3 was found to be a more potent inhibitor of HIV-1 replication than C1 and C2 (Fig. 3C). Its EC_{50} was 617 ± 11 nM (Table 1). C3 also inhibited HIV-1 replication in TNF-α-stimulated U1 cells, with an EC_{50} of 168 ± 97 nM (Fig. 3D). C3 reduced the viability of OM-10.1 and U1 cells by 53 and 56% of that of the control cells at the concentration of 10,000 nM, respectively (Fig. 3C and D). The selective indices (SIs), based on the ratio of the 50% cytotoxic concentration (CC_{50}) to the EC_{50}, were more than 16 and 60 in OM-10.1 and U1 cells, respectively (Table 1).

TABLE 1 Anti-HIV-1 activity of C3 on chronically and acutely HIV-1-infected cells[a]

Cell type	Infection type	TNF-α	EC_{50}[b] (nM)	CC_{50}[c] (nM)	SI[d]
OM-10.1	Chronic	+	617 ± 11	>10,000	>16
U1	Chronic	+	168 ± 97	>10,000	>60
CEM	Acute	−	19.9 ± 3.4	>1,000	>50
MOLT-4	Acute	−	17.9 ± 6.6	>1,000	>55
PBMCs	Acute	−	9.6	6,800	708

[a] All data represent means ± standard deviations for three separate experiments.
[b] The EC_{50} inhibits the level of p24 antigen in culture supernatants by 50%.
[c] The CC_{50} reduces the viability of non-TNF-α-treated OM-10.1 cells and U1 cells or mock-infected CEM cells, MOLT-4 cells, and PBMCs by 50%.
[d] The SI is based on the ratio of the CC_{50} to the EC_{50}.

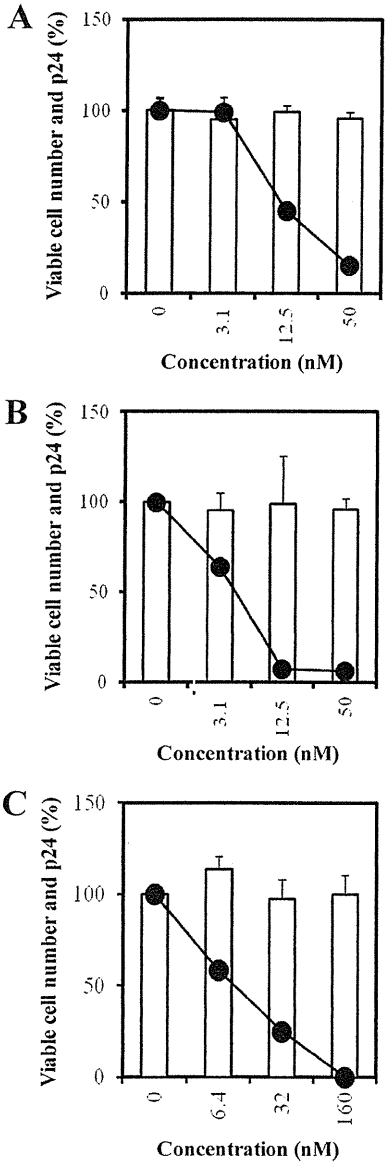

FIG 4 Anti-HIV-1 activity of C3 in acutely infected cells. CEM (A) and MOLT-4 (B) cells were infected with HIV-1 at an MOI of 0.001, and PBMCs (C) were infected with HIV-1 at an MOI of 0.01. The infected cells were incubated in the presence of various concentrations of the compound. After incubation for 72 h, the cells were subcultured and further incubated for 72 h. The p24 levels in the culture supernatants (circles with line) and cell viability (bars) were determined by ELISA and the MTT method, respectively. Data are expressed as the percentage of the control (p24 level and viable cell number in the absence of compounds). All experiments were carried out in duplicate, and mean values and standard errors are shown.

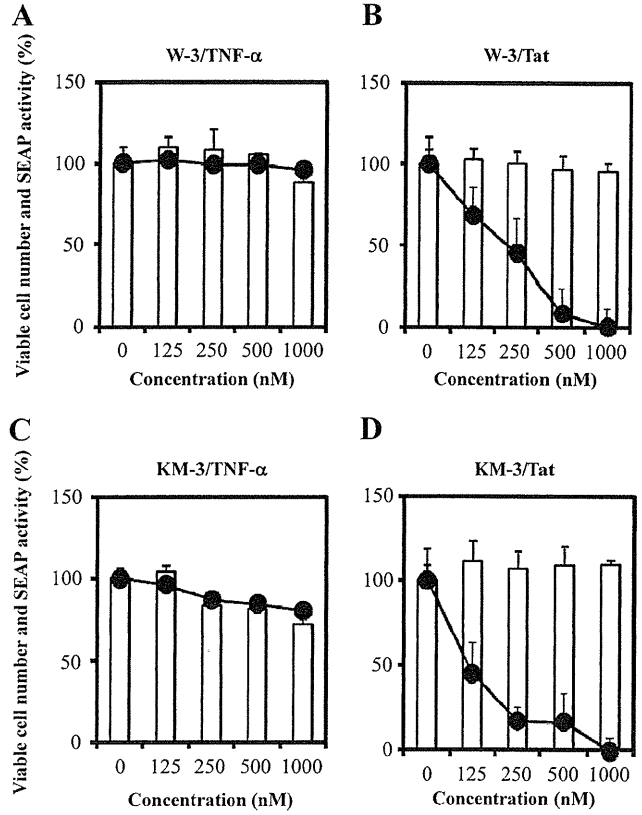

FIG 5 Inhibitory effect of C3 on Tat-mediated transcription. W-3 (A and B) and KM-3 (C and D) cells were treated with TNF-α (A and C) or transfected with the Tat expression plasmid (B and D). The cells were cultured in the presence of various concentrations of the compound. After incubation for 24 h, the culture supernatants were collected and examined for their SEAP levels (circles with line). The viable cell number (bars) was determined by the MTT method. Data are expressed as the percentage of the control (SEAP level and viable cell number in the absence of compounds). All experiments were carried out in duplicate, and means values and standard errors are shown.

In the next experiment, the anti-HIV-1 activity of C3 was examined in CEM cells, MOLT-4 cells, and PBMCs, all of which were acutely infected with HIV-1. As shown in Fig. 4, C3 selectively inhibited HIV-1 replication, irrespective of the cells used for assays. Its EC_{50}s were 19.9 ± 3.4 nM for CEM cells and 17.9 ± 6.6 nM for MOLT-4 cells, while the CC_{50}s were more than 1,000 nM in both cell lines. Thus, the SIs were more than 50 and 55 in CEM and MOLT-4 cells, respectively (Table 1). When the cytotoxicity of C3 was determined after 3 weeks of cultivation, its CC_{50} was found to be unchanged (data not shown). Furthermore, C3 inhibited HIV-1 replication in PBMCs, with an EC_{50} of 9.6 nM. Since its CC_{50} for PBMCs was 6,800 nM, the SI was 708. C3 was also active against HIV-2 replication. Its EC_{50}s against HIV-2 (ROD strain) were 136.5 ± 7.9 and 110.5 ± 2.7 nM in CEM and MOLT-4 cells, respectively (data not shown).

Inhibitory effect on Tat-mediated transcription. To gain insight into the mechanism of action, C3 was examined for its inhibitory effect on NF-κB- or Tat-mediated HIV-1 LTR-driven gene expression in reporter cells. W-3 cells are reactive to stimulation with both TNF-α and Tat, since the cells carry a reporter (SEAP) gene with two intact NF-κB-binding sites in the HIV-1 LTR as a promoter. In contrast, KM-3 cells having two mutated NF-κB-binding sites are not reactive to TNF-α but are fully reactive to Tat. In the absence of C3, TNF-α induced an approximately 4-fold increase in SEAP activity in the culture supernatants of W-3 cells, but no such increase in SEAP activity was observed in KM-3 cells (data not shown). On the other hand, transfection with the Tat expression plasmid induced a 4-fold increase in SEAP activity in both W-3 and KM-3 cells (data not shown). Although C3 did not affect the SEAP activity of the culture supernatants of TNF-α-treated W-3 cells (Fig. 5A), a dose-dependent decrease in SEAP

TABLE 2 Effect of C3 on TNF-α- or Tat-induced HIV-1 LTR transactivation[a]

Cell type	Tat	TNF-α	EC_{50}[b] (nM)	CC_{50}[c] (nM)
W-3	+	−	183 ± 50	>2,000
	−	+	>2,000	>2,000
KM-3	+	−	107 ± 11	>2,000
	−	+	>2,000	>2,000

[a] All data represent means ± standard deviations for three separate experiments.
[b] EC_{50}, 50% effective concentration, i.e., concentration that inhibits SEAP activity in culture supernatants by 50%.
[c] The CC_{50} reduces the cell viability by 50%.

activity was observed in W-3 and KM-3 cells transfected with the Tat expression plasmid (Fig. 5B and D). The EC_{50}s of C3 for SEAP were 183 ± 50 nM for W-3 cells and 107 ± 11 nM for KM-3 cells. Its CC_{50}s were more than 2,000 nM in both cell lines (Table 2). These results indicate that C3 specifically inhibited Tat-mediated HIV-1 LTR-driven transcription.

Inhibitory effect on Tat-induced phosphorylation of RNAPII. HIV-1 Tat recruits P-TEFb (CDK9/CycT1) to TAR RNA on nascent HIV-1 transcripts, and the CDK9 subunit of P-TEFb phosphorylates Ser2 on the heptad repeats in the CTD of RNAPII

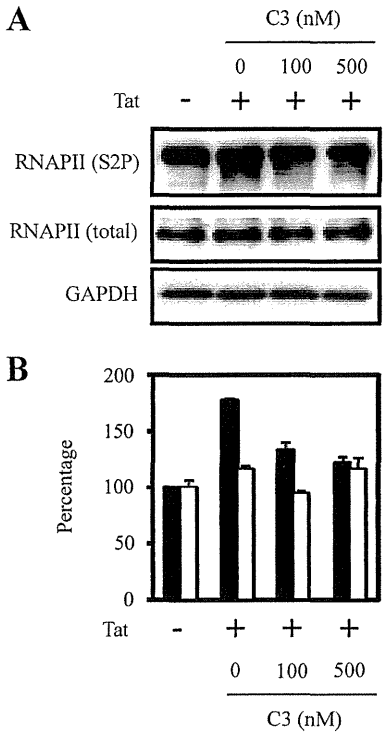

FIG 6 Inhibitory effects of C3 on Tat-induced phosphorylation of RNAPII. W-3 cells were transfected with the Tat expression plasmid and cultured in the presence of various concentrations of the compound. After incubation for 48 h, the whole-cell lysates were subjected to Western blot analysis with anti-phosphorylated RNAPII (Ser2), anti-RNAPII, and anti-GAPDH antibodies. Panels A and B show the bands of blots and the amounts of phosphorylated RNAPII (Ser2P) (solid bars) and total RNAPII (open bars), both of which were normalized by the amount of GAPDH as a control. The levels of phosphorylated RNAPII and total RNAPII in W-3 cells without plasmid transfection are expressed as 100%. The experiments were performed twice, and the data represent means ± ranges for two separate experiments.

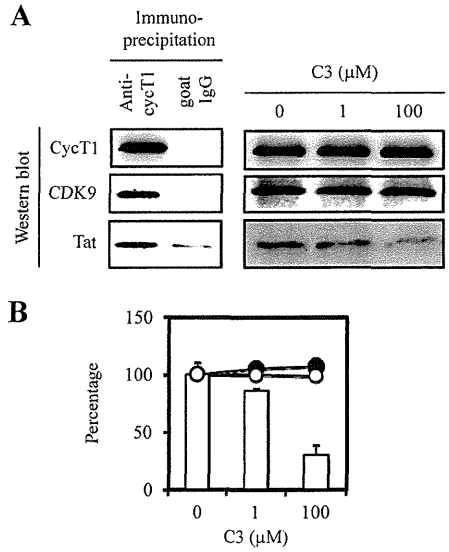

FIG 7 Inhibitory effects of C3 on Tat-CycT1 interaction. CycT1 from a CEM cell lysate was incubated with Tat in the presence of various concentrations of C3. After incubation for 2 h, the samples were subjected to Western blot analysis with anti-CycT1, anti-CDK9, and anti-Tat antibodies. (A) The left panel shows the samples precipitated with anti-CycT1 antibody- or goat IgG-immobilized beads in the absence of compound. The right panel shows the samples precipitated with anti-CycT1 antibody-immobilized beads in the absence or presence of the compound. (B) The amounts of CycT1 (solid circles), CDK9 (open circles), and Tat (bars) were determined photodensitometrically, and those in the absence of the compound are expressed as 100%. The data represent means ± ranges for two separate experiments.

to induce HIV-1 transcription (6, 9, 10). To investigate the inhibitory effect of C3 on phosphorylation of Ser2 during transcription, Western blot analysis was conducted for the lysate from W-3 cells which had been transfected with the Tat expression plasmid and cultured in the presence of C3. While the phosphorylation of Ser2 was detected in the absence of Tat, the transfection with the Tat expression plasmid augmented the phosphorylation 1.7-fold (Fig. 6). When the cells were exposed to C3, the phosphorylation of Ser2 was suppressed in a dose-dependent fashion without affecting the total RNAPII protein level (Fig. 6). These results suggest that C3 suppresses Tat-induced phosphorylation of RNAPII and inhibits HIV-1 transcription before transition from the initiation step to the elongation step.

Inhibitory effect on CycT1-Tat interaction. When the binding assay between Tat and CycT1 was conducted in the absence of C3, Tat could bind to CycT1 purified from CEM cells with anti-CycT1 antibody beads. Although Tat nonspecifically bound to goat IgG beads in this assay, the binding level was low. In the presence of C3, the binding of Tat to CycT1 was inhibited by C3 in a dose-dependent fashion, whereas the levels of CDK9 and CycT1 were not affected by the compound (Fig. 7). These results suggest that C3 specifically targets the interaction between Tat and CycT1.

Docking pose to CycT1. To define the docking pose of C3, we recalculated the docking energy and found two stable docking poses, docking pose 1 (Fig. 8A) and docking pose 2 (Fig. 8B). Docking pose 1 demonstrated that methoxyquinolone, pyridine, and benzothiadiazole moieties of C3 were located on target sites 1, 2, and 3 in CycT1, respectively (Fig. 8A), while they were located

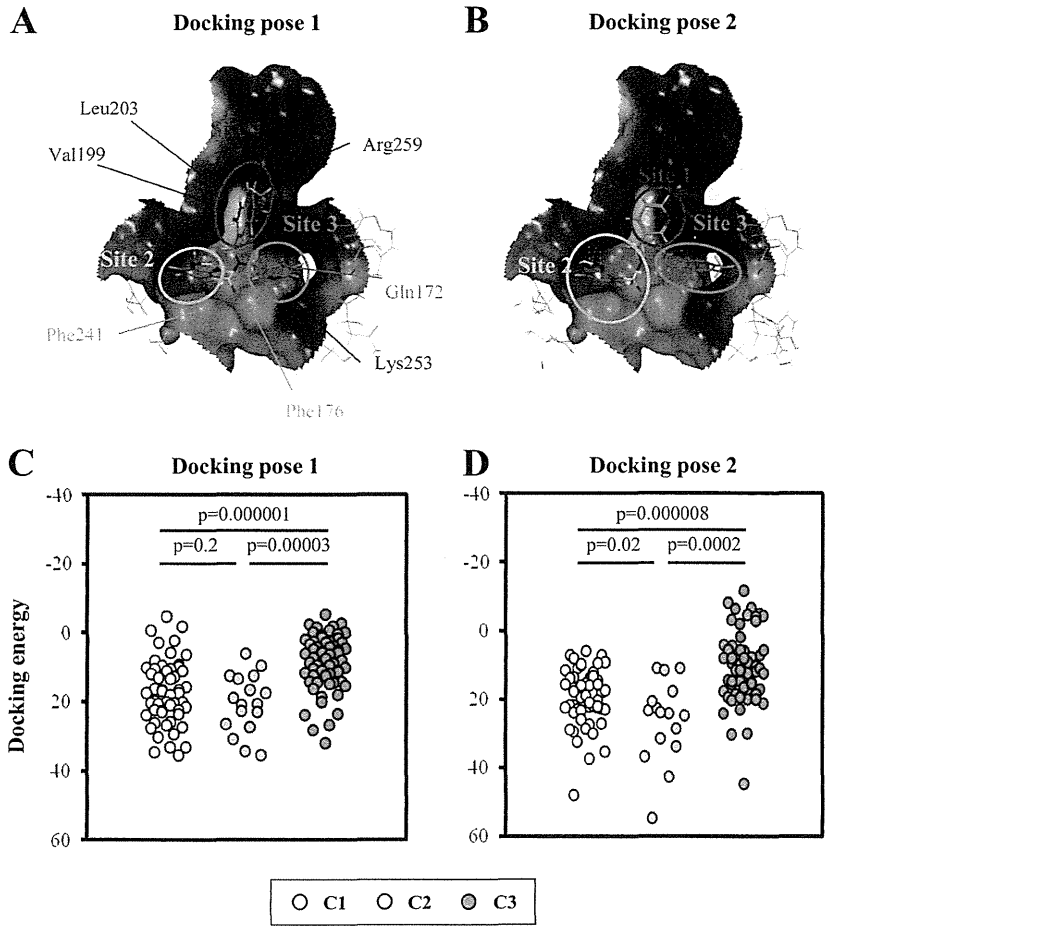

FIG 8 Docking poses of C3 to CycT1. Docking pose 1 (A) and docking pose 2 (B) of C3 are indicated in the model structure of human CycT1. Sites 1, 2, and 3 in the target region for *in silico* screening are shown in red, yellow, and blue, respectively. Docking energies of C1 to C3 with human CycT1 in docking pose 1 (C) and docking pose 2 (D) were compared. Statistical significance was determined by Student's *t* test.

on the sites 2, 1, and 3, respectively, in the docking pose 2 (Fig. 8B). When the docking energy of C1 to C3 was evaluated in docking pose 1, the docking energy of C3 was significantly stronger than those of C1 and C2 (Fig. 8C). However, no significant difference of docking energy was observed between C1 and C2. Thus, the result on docking pose 1 was consistent with that for their anti-HIV-1 activity (C3 > C1 = C2). In docking pose 2, the docking energy was found to differ significantly between C1 and C2 (Fig. 8D), which was inconsistent with their anti-HIV-1 activity. Thus, docking pose 1 is more appropriate to explain the interaction between C3 and CycT1. In docking pose 1, C3 had direct interaction with Val199, Leu203, Phe241, Lys253, and Arg259 and was located near Gln172 and Phe176 of CycT1.

DISCUSSION

In this work, we describe a novel class of anti-HIV-1 compounds obtained by *in silico* screening targeting the TRM of CycT1. Although the transcription process of HIV-1 has not fully been exploited for therapeutic intervention yet, this process plays a crucial role in viral replication. In spite of various attempts to develop HIV-1 transcription inhibitors (32, 33), none of the inhibitors have successfully been approved for clinical use because of their potential toxicity. Since the transcription process of HIV-1 involves several host cellular factors, these compounds most likely inhibited these host factors. To circumvent such a problem, our strategy for identifying transcription inhibitors was to introduce *in silico* screening of compounds targeting the TRM. Although CycT1 is a host factor essential for cellular functions, the TRM is considered to be a unique interface for Tat and TAR RNA binding.

Using *in silico* screening followed by *in vitro* anti-HIV-1 assay, we found two structurally related compounds (C1 and C2) that acted as selective inhibitors of HIV-1 replication in TNF-α-stimulated OM-10.1 cells (Fig. 3A and B). We also identified C3 as a more potent inhibitor than C1 and C2 by further screening. C3 inhibited HIV-1 replication not only in chronically infected cells (OM-10.1 and U1 cells) but also in acutely infected cells (CEM and MOLT-4 cells and PBMCs) (Table 1). Since Tat strongly induces HIV-1 transcription through the phosphorylation of RNAPII after recruiting the CDK9/CycT1 complex to the HIV-1 LTR (6–10), we examined the inhibitory effect of C3 on this process. Using a reporter expression cell system regulated under the control of the HIV-1 LTR, C3 was found to inhibit Tat-induced reporter (SEAP) expression (Fig. 5). In addition, C3 also inhibited the phosphorylation of Ser2 in the CTD of RNAPII (Fig. 6) and the binding of Tat to CycT1 (Fig. 7) *in vitro*. Thus, the inhibitory effect

of C3 on HIV-1 replication is probably due to the impairment of CycT1/CDK9/Tat/TAR RNA complex formation.

Although the three-dimensional structure of the human CycT1/HIV-1 Tat/TAR RNA complex has not fully been clarified, two structures, equine CycT1/EIAV Tat/TAR RNA (14) and human CycT1/HIV-1 Tat (15), are currently available for structure-based drug design. Since the TRM of CycT1 interacts with both Tat and TAR RNA, this region is important for complex formation and is an attractive target for inhibition of HIV-1 replication. Since the structure of human CycT1/HIV-1 Tat complex lacks the information of the TRM, we used the equine CycT1/EIAV Tat/TAR RNA complex as a model structure of human CycT1 for *in silico* screening. The TRM of equine CycT1 directly interacts with EIAV Tat, and the amino acids involved in this interaction are highly conserved in human CycT1 and HIV-1 Tat. However, unlike HIV-1 TAR RNA, EIAV TAR RNA is located far from the TRM of equine CycT1, according to the crystallographic structure of the equine CycT1/EIAV Tat/TAR RNA complex. It is possible that conformational change of the TRM of equine CycT1 is induced solely by Tat binding and not by TAR RNA binding. Therefore, in spite of the possible lack of interaction between the TRM of equine CycT1 and EIAV TAR RNA, we could identify C3 as a novel inhibitor of HIV-1 transcription by *in silico* screening. These results suggest that the TRM model based on the structure of the equine CycT1/EIAV Tat/TAR RNA complex adequately mimics the actual structure of the TRM of human CycT1 with viral factors.

In a previous study, we conducted *in silico* screening of compounds targeting a site containing the TRM of human CycT1 fused with EIAV Tat (PDB ID: 2PK2) (34). Using this system, we identified three compounds that inhibited HIV-1 replication in acutely infected cells at submicromolar concentrations (unpublished data). However, these compounds did not show any anti-HIV-1 activity in chronically infected cells, indicating that the compounds inhibit an early step in the viral life cycle and that the crystal structure of human CycT1 fused with EIAV Tat is not suitable as a model for *in silico* screening. Although the amino acids of the target site were not completely identical between the previous study and this study, both of them included the TRM. Therefore, the addition of TAR RNA to the CycT1/Tat complex seems to indirectly alter the conformation of the TRM, and this alteration may be important in identifying HIV-1 transcription inhibitors by *in silico* screening.

To define the docking pose of C3 with CycT1, we conducted docking studies of compounds and found a suitable docking pose of C3, where the *in vitro* anti-HIV-1 activity of the compounds was correlated with their *in silico* docking energy (Fig. 8). In fact, all of the inactive compounds (C4 to C10 in Fig. 2) did not bind to CycT1 *in silico* (data not shown). The best docking pose revealed that C3 interacted with V199, L203, F241, K253, and R259 and was near the surface of Q172 and F176 of CycT1. Since Q172, F176, and R259 of human CycT1 interact with HIV-1 Tat, these amino acids appear to be particularly important for the anti-HIV-1 activity of C3. Consequently, this docking pose and structure-activity relationship of the series of compounds may provide useful information on design for more effective inhibitors.

In conclusion, the *in silico* screening system described herein is a useful tool for investigating novel inhibitors that target the TRM of human CycT1, and C3 identified in this system is considered to be a promising lead for novel HIV-1 transcription inhibitors.

ACKNOWLEDGMENTS

This study was supported in part by a research grant from the Ministry of Health, Labor, and Welfare of Japan.

REFERENCES

1. Volberding PA, Deeks SG. 2010. Antiretroviral therapy and management of HIV infection. Lancet 376:49–62.
2. Pierson T, McArthur J, Siliciano RF. 2000. Reservoirs for HIV-1: mechanisms for viral persistence in the presence of antiviral immune responses and antiretroviral therapy. Annu. Rev. Immunol. 18:665–708.
3. Letvin NL. 2009. Virology. Moving forward in HIV vaccine development. Science 326:1196–1198.
4. Barboric M, Peterlin BM. 2005. A new paradigm in eukaryotic biology: HIV Tat and the control of transcriptional elongation. PLoS Biol. 3:e76. doi:10.1371/journal.pbio.0030076.
5. Marciniak RA, Sharp PA. 1991. HIV-1 Tat protein promotes formation of more-processive elongation complexes. EMBO J. 10:4189–4196.
6. Peterlin BM, Price DH. 2006. Controlling the elongation phase of transcription with P-TEFb. Mol. Cell 23:297–305.
7. Wei P, Garber ME, Fang SM, Fischer WH, Jones KA. 1998. A novel CDK9-associated C-type cyclin interacts directly with HIV-1 Tat and mediates its high-affinity, loop-specific binding to TAR RNA. Cell 92:451–462.
8. Bannwarth S, Gatignol A. 2005. HIV-1 TAR RNA: the target of molecular interactions between the virus and its host. Curr. HIV Res. 3:61–71.
9. Karn J. 1999. Tackling Tat. J. Mol. Biol. 293:235–254.
10. Price DH. 2000. P-TEFb, a cyclin-dependent kinase controlling elongation by RNA polymerase II. Mol. Cell. Biol. 20:2629–2634.
11. Peng J, Zhu Y, Milton JT, Price DH. 1998. Identification of multiple cyclin subunits of human P-TEFb. Genes Dev. 12:755–762.
12. Fujinaga K, Taube R, Wimmer J, Cujec TP, Peterlin BM. 1999. Interactions between human cyclin T, Tat, and the transactivation response element (TAR) are disrupted by a cysteine to tyrosine substitution found in mouse cyclin T. Proc. Natl. Acad. Sci. U. S. A. 96:1285–1290.
13. Garber ME, Wei P, KewalRamani VN, Mayall TP, Herrmann CH, Rice AP, Littman DR, Jones KA. 1998. The interaction between HIV-1 Tat and human cyclin T1 requires zinc and a critical cysteine residue that is not conserved in the murine CycT1 protein. Genes Dev. 12:3512–3527.
14. Anand K, Schulte A, Vogel-Bachmayr K, Scheffzek K, Geyer M. 2008. Structural insights into the cyclin T1-Tat-TAR RNA transcription activation complex from EIAV. Nat. Struct. Mol. Biol. 15:1287–1292.
15. Tahirov TH, Babayeva ND, Varzavand K, Cooper JJ, Sedore SC, Price DH. 2010. Crystal structure of HIV-1 Tat complexed with human P-TEFb. Nature 465:747–751.
16. Cecchetti V, Parolin C, Moro S, Pecere T, Filipponi E, Calistri A, Tabarrini O, Gatto B, Palumbo M, Fravolini A, Palu G. 2000. 6-Aminoquinolones as new potential anti-HIV agents. J. Med. Chem. 43:3799–3802.
17. Chao SH, Fujinaga K, Marion JE, Taube R, Sausville EA, Senderowicz AM, Peterlin BM, Price DH. 2000. Flavopiridol inhibits P-TEFb and blocks HIV-1 replication. J. Biol. Chem. 275:28345–28348.
18. Davidson A, Leeper TC, Athanassiou Z, Patora-Komisarska K, Karn J, Robinson JA, Varani G. 2009. Simultaneous recognition of HIV-1 TAR RNA bulge and loop sequences by cyclic peptide mimics of Tat protein. Proc. Natl. Acad. Sci. U. S. A. 106:11931–11936.
19. Wang D, de la Fuente C, Deng L, Wang L, Zilberman I, Eadie C, Healey M, Stein D, Denny T, Harrison LE, Meijer L, Kashanchi F. 2001. Inhibition of human immunodeficiency virus type 1 transcription by chemical cyclin-dependent kinase inhibitors. J. Virol. 75:7266–7279.
20. Baba M, Okamoto M, Kawamura M, Makino M, Higashida T, Takashi T, Kimura Y, Ikeuchi T, Tetsuka T, Okamoto T. 1998. Inhibition of human immunodeficiency virus type 1 replication and cytokine production by fluoroquinoline derivatives. Mol. Pharmacol. 53:1097–1103.
21. Wang X, Yamataka K, Okamoto M, Ikeda S, Baba M. 2007. Potent and selective inhibition of Tat-dependent HIV-1 replication in chronically infected cells by a novel naphthalene derivative JTK-101. Antivir. Chem. Chemother. 18:201–211.
22. Butera ST, Perez VL, Wu BY, Nabel GJ, Folks TM. 1991. Oscillation of

the human immunodeficiency virus surface receptor is regulated by the state of viral activation in a CD4+ cell model of chronic infection. J. Virol. 65:4645–4653.
23. **Folks TM, Justement J, Kinter A, Dinarello CA, Fauci AS.** 1987. Cytokine-induced expression of HIV-1 in a chronically infected promonocyte cell line. Science 238:800–802.
24. **Kikukawa R, Koyanagi Y, Harada S, Kobayashi N, Hatanaka M, Yamamoto N.** 1986. Differential susceptibility to the acquired immunodeficiency syndrome retrovirus in cloned cells of human leukemic T-cell line Molt-4. J. Virol. 57:1159–1162.
25. **Baba M, Okamoto M, Takeuchi H.** 1999. Inhibition of human immunodeficiency virus type 1 replication in acutely and chronically infected cells by EM2487, a novel substance produced by a Streptomyces species. Antimicrob. Agents Chemother. 43:2350–2355.
26. **Halgren TA.** 1999. MMFF VI. MMFF94s option for energy minimization studies. J. Comput. Chem. 20:720–729.
27. **Halgren TA.** 1999. MMFF VII. Characterization of MMFF94, MMFF94s, and other widely available force fields for conformational energies and for intermolecular-interaction energies and geometries. J. Comput. Chem. 20:730–748.
28. **Weiner SJ, Kollman PA, Case DA, Singh UC, Ghio C, Alagona G, Profeta S, Weiner P.** 1984. A new force field for molecular mechanical simulation of nucleic acids and proteins. J. Am. Chem. Soc. 106:765–784.
29. **Goto J, Kataoka R, Muta H, Hirayama N.** 2008. ASEDock-docking based on alpha spheres and excluded volumes. J. Chem. Inf. Model. 48:583–590.
30. **Pauwels R, Balzarini J, Baba M, Snoeck R, Schols D, Herdewijn P, Desmyter J, De Clercq E.** 1988. Rapid and automated tetrazolium-based colorimetric assay for the detection of anti-HIV compounds. J. Virol. Methods 20:309–321.
31. **Chou TC, Talalay P.** 1987. Applications of the median-effect principle for the assessment of low-dose risk of carcinogens and for the quantitation of synergism and antagonism of chemotherapeutic agents, p 37–64. *In* Harrap KR, Connors TA (ed), New avenues in developmental cancer chemotherapy. Bristol-Myers symposium series. Academic Press, New York, NY.
32. **Baba M.** 2006. Recent status of HIV-1 gene expression inhibitors. Antiviral Res. 71:301–306.
33. **Stevens M, De Clercq E, Balzarini J.** 2006. The regulation of HIV-1 transcription: molecular targets for chemotherapeutic intervention. Med. Res. Rev. 26:595–625.
34. **Anand K, Schulte A, Fujinaga K, Scheffzek K, Geyer M.** 2007. Cyclin box structure of the P-TEFb subunit cyclin T1 derived from a fusion complex with EIAV tat. J. Mol. Biol. 370:826–836.

Chemistry & Biology
Article

CXCR4 Stimulates Macropinocytosis: Implications for Cellular Uptake of Arginine-Rich Cell-Penetrating Peptides and HIV

Gen Tanaka,[1] Ikuhiko Nakase,[1] Yasunori Fukuda,[1] Ryo Masuda,[2] Shinya Oishi,[2] Kazuya Shimura,[4] Yoshimasa Kawaguchi,[1] Tomoka Takatani-Nakase,[5] Ülo Langel,[6] Astrid Gräslund,[7] Katsuya Okawa,[3,9] Masao Matsuoka,[4] Nobutaka Fujii,[2] Yasumaru Hatanaka,[8] and Shiroh Futaki[1,*]

[1]Institute for Chemical Research, Kyoto University, Uji, Kyoto 611-0011, Japan
[2]Graduate School of Pharmaceutical Sciences
[3]Frontier Technology Center, Kyoto University Faculty of Medicine
Kyoto University, Sakyo-ku, Kyoto 606-8501, Japan
[4]Institute for Virus Research, Kyoto University, Sakyo-ku, Kyoto 606-8507, Japan
[5]School of Pharmaceutical Sciences, Mukogawa Women's University, Nishinomiya, Hyogo 663-8179, Japan
[6]Department of Neurochemistry, Stockholm University, 106 92 Stockholm, Sweden
[7]Department of Biochemistry and Biophysics, Arrhenius Laboratories for Natural Sciences, Stockholm University, 106 91 Stockholm, Sweden
[8]Graduate School of Medicine and Pharmaceutical Sciences, University of Toyama, Sugitani, Toyama 930-0194, Japan
[9]Present address: Drug Discovery Research Laboratories, Kyowa Hakko Kirin, Nagaizumi-cho, Suntou-gun, Shizuoka 411-8731, Japan
*Correspondence: futaki@scl.kyoto-u.ac.jp
http://dx.doi.org/10.1016/j.chembiol.2012.09.011

SUMMARY

CXCR4 is a coreceptor of HIV-1 infection in host cells. Through a photocrosslinking study to identify receptors involved in internalization of oligoarginine cell-penetrating peptides (CPPs), we found that CXCR4 serves as a receptor that stimulates macropinocytic uptake of the arginine 12-mer peptide (R12) but not of the 8-mer. We also found that stimulating CXCR4 with its intrinsic ligands, stromal cell-derived factor 1α and HIV-1 envelope glycoprotein 120, induced macropinocytosis. R12 had activity to prevent viral infection for HIV-1_{IIIB}, a subtype of HIV-1 that uses CXCR4 as a coreceptor for entry into susceptible cells, whereas the addition of a macropinocytosis inhibitor, dimethylamiloride, resulted in enhancement of viral infection. The present study shows that CXCR4 triggers macropinocytosis, which may have implications for the cellular uptake of oligoarginine CPPs and internalization of HIV.

INTRODUCTION

Recently developed intracellular delivery technology using cell-penetrating peptides (CPPs) has provided novel strategies for drug delivery, diagnostics, and chemical biology (Futaki, 2006; Wender et al., 2008). Conjugation of CPPs to molecules of interest leads to the efficient delivery of these molecules into cells, and successful modulation of cellular function has been reported. Arginine-rich CPPs, including oligoarginines and one derived from positions 48–60 of HIV-1 Tat protein (Tat peptide), are a representative CPP class (Futaki, 2006). Understanding the internalization methods of these CPPs and their conjugates should be beneficial for the design of more sophisticated and effective delivery systems. However, there remain many ambiguities regarding their methods of internalization.

It has been demonstrated by our group and others that macropinocytosis also plays an important part in the cellular uptake of arginine-rich CPPs to achieve high-efficiency intracellular delivery (Nakase et al., 2004; Wadia et al., 2004). Macropinocytosis is a transient, actin-driven fluid-phase endocytosis that involves membrane ruffling and the formation of large vacuoles called macropinosomes (Swanson and Watts, 1995; Conner and Schmid, 2003; Falcone et al., 2006). In most cells other than dendritic cells, macropinocytosis is not a constitutive endocytosis process but rather is activated by external stimuli such as epidermal growth factors and fibroblast growth factor 2 (FGF2) (Tkachenko et al., 2004). Ruffling of plasma membranes is induced by actin reorganization (Meier et al., 2002). Protrusion of the plasma membranes, followed by membrane fusion, leads to the formation of large endocytic vacuoles with a diameter that often exceeds 1 μm (Conner and Schmid, 2003). The importance of this endocytic pathway to the infection of various viruses has recently received attention (Mercer and Helenius, 2008, 2009).

On the other hand, CXCR4 is a CXC chemokine receptor (C-X-C chemokine receptor type 4) and is also a coreceptor for HIV-1 infection. Binding of HIV-1 envelope glycoprotein 120 (gp120) to CD4 host cells leads to further interactions with CXCR4 and the eventual fusion of viral and host cell membranes driven by the HIV-1 gp41 protein (Tamamura et al., 2005). CXCR4 is thus a promising target for anti-HIV agents (Schramm et al., 2000). Stromal cell-derived factor 1α (SDF-1α) is a natural CXCR4 ligand. Induction of CXCR4 endocytosis and actin polymerization by SDF-1α has been suggested (Rey et al., 2007; Yoder et al., 2008). It has been reported that SDF-1α induces rapid endocytosis and downmodulation of CXCR4 (Signoret et al., 1997; Orsini et al., 1999; Venkatesan et al., 2003). It has also been reported that treatment of cells with SDF-1α leads to actin polymerization (Rey et al., 2007; Yoder et al., 2008). However, although involvement of clathrin-dependent endocytosis has

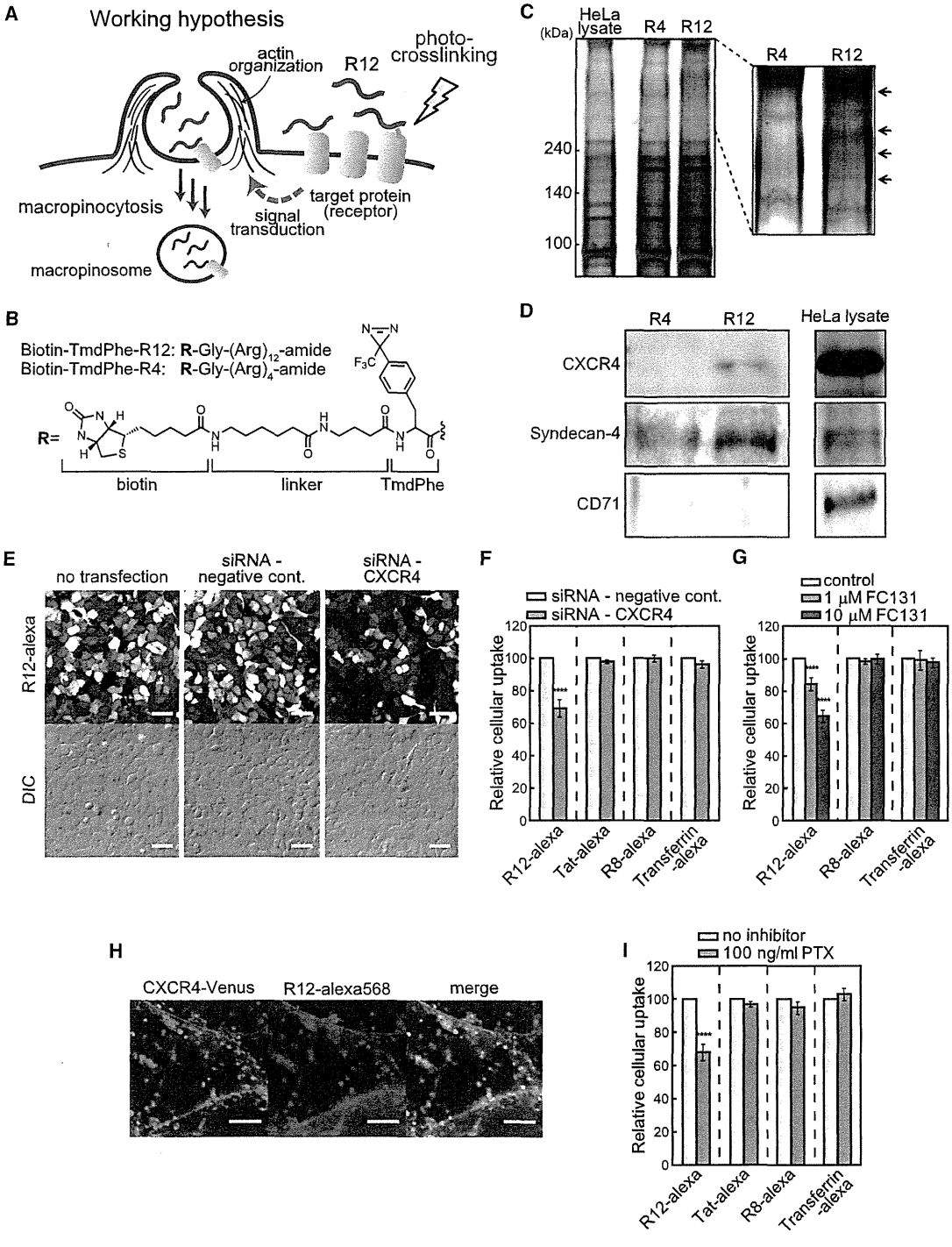

Figure 1. Identification of CXCR4 as a Potential Receptor that Contributes to Cellular Uptake of the Arginine R12 Peptide

(A) Outline of the photocrosslinking study to identify the cell-surface receptor for the R12 peptide.

(B) Structure of biotin-TmdPhe-R12, the photocrosslinking probe to identify the receptor responsible for R12 cellular uptake. Structures of other peptides used in this study are given in Figure S3.

(C) SDS-PAGE of the proteins obtained with magnetic spheres after photocrosslinking of HeLa cells with biotin-TmdPhe-R12 (0.5 μM) or biotin-TmdPhe-R4 (1.5 μM) for 3 min at 4°C. Arrows indicate specific bands observed for biotin-TmdPhe-R12-treated cells.

(D) Western blot analysis of the proteins obtained with magnetic spheres from biotin-TmdPhe-R12-treated cells yielded positive staining with the anti-CXCR4 antibody but not with the anti-CD71 antibody.

been suggested, no direct evidence has been reported indicating that SDF-1α induces macropinocytosis.

In this report, we synthesized dodeca-arginine (R12) bearing the phenyltrifluoromethyldiazirine moiety as a photocrosslinker with the hope of identifying the receptors responsible for the cellular uptake of oligoarginines (Figure 1A). We found that CXCR4 is a receptor that stimulates cellular uptake of the R12 peptide. Binding of R12 to CXCR4 stimulates actin organization and macropinocytosis. The binding of R12 to CXCR4 also leads to CXCR4 internalization. We also found that stimulating CXCR4 with its natural ligands, SDF-1α or gp120, triggered macropinocytosis together with internalization of the receptor. These results thus shed light on the roles of CXCR4 as a receptor for stimulating cellular uptake of arginine-rich CPPs and the induction of macropinocytosis, which may have implications in cellular responses, accompanied by intracellular delivery using oligoarginines, and in HIV infection.

RESULTS

CXCR4 as a Potential Target of R12 on Plasma Membranes

Photocrosslinking is a powerful methodology to detect molecular interactions in cells (Tomohiro et al., 2005). A biotin-tagged R12 peptide bearing trifluoromethyldiazirinephenylalanine (biotin-TmdPhe-R12) was designed to identify cell-surface molecules that can be recognized by the R12 peptide (Figure 1B). The R12 peptide was selected as a typical arginine-rich CPP with superior internalization efficiency, compared with the R8 and Tat peptides (Kosuge et al., 2008). Aryl-3-phenyl-3-trifluoromethyldiazirine derivatives are effective photocrosslinking agents and are readily incorporated into peptide chains using trifluoromethyldiazirinephenylalanine derivatives developed by Hatanaka and coworkers (Nakashima et al., 2006). The biotin tag was incorporated at the N terminus of the peptide together with a flexible linker (γ-aminobutyric acid) to facilitate the isolation of crosslinked proteins with the TmdPhe-R12 peptide. The biotin-TmdPhe-R12 peptide was thus prepared by Fmoc solid-phase peptide synthesis without difficulty.

HeLa cells pretreated with 0.5 μM biotin-TmdPhe-R12 at 37°C for 30 s were irradiated with UV light (365 nm) at 4°C for 3 min and washed with PBS prior to cell lysis. The peptide concentration and incubation time were set so that the peptide interacted with cell-surface molecules, but no significant endocytosed peptide signal was observed after examining the time course and the FITC-TmdPhe-R12 internalization methods (see Figure S1A available online). The biotin-TmdPhe-R4 peptide was used as a negative control; the R4 peptide showed no significant internalization (Futaki et al., 2001; Kosuge et al., 2008). After dialysis at 4°C for 12 hr, the samples were treated with streptavidin magnetic spheres for 1 hr. Proteins crosslinked with the R12 peptide were collected and the samples were subjected to SDS-PAGE (Figure 1C). Proteins corresponding to four major bands >240 kDa were specifically observed from cells treated with biotin-TmdPhe-R12 (arrows in Figure 1C) compared with those treated with biotin-TmdPhe-R4, and were digested with trypsin. The digested peptides were analyzed by MALDI-TOF mass spectrometry (MS) with peptide mass fingerprinting (PMF), and it was determined that the four bands were derived from myosin-9 (nonmuscle myosin heavy chain IIA). Involvement of myosin-9 in the endocytosis of CXCR4 and their colocalization on the cell surface, together with cell-surface exposure of myosin-9, has been suggested previously (Rey et al., 2007; Arii et al., 2010). Additionally, CXCR4 is expressed on the cell surface in a complex with syndecan-4 (Hamon et al., 2004). A western blot analysis of the proteins obtained using magnetic spheres from biotin-TmdPhe-R12-treated cells yielded positive staining with an anti-CXCR4 antibody, whereas no significant staining was observed for samples from biotin-TmdPhe-R4-treated cells (Figure 1D). Similarly, positive staining with anti-syndecan-4 antibody was observed for samples obtained from biotin-TmdPhe-R12-treated cells, which was almost twice as strong as that from biotin-TmdPhe-R4-treated cells (Figure 1D). These results suggest the possibility that CXCR4 plays a role in the cell-surface recognition of biotin-TmdPhe-R12.

CXCR4 as a Receptor to Promote R12 Uptake

The involvement of CXCR4 in the cellular uptake of R12 was then confirmed using CXCR4-knockdown HeLa cells, expressing 48% decreased levels of the receptor (Figure S1B). A significant decrease in R12-Alexa fluorescence signals was observed in the CXCR4-knockdown cells (Figure 1E, right) versus that in non-treated cells (Figure 1E, left) or in cells treated with negative-control siRNA (Figure 1E, middle). Fluorescence-activated cell sorting analysis showed a considerable decrease (32%) in the cellular uptake of the R12 peptide by CXCR4 knockdown under the same conditions (Figure 1F). Treating HeLa cells with the CXCR4-specific antagonist FC131 (cyclo[-D-Tyr-Arg-Arg-Nal-Gly-]) (Fujii et al., 2003) (10 μM) also resulted in a decrease in R12 peptide cellular uptake (Figure 1G). These results suggest the involvement of CXCR4 in the cellular uptake of R12.

(E and F) Downregulation of CXCR4 led to diminished cellular uptake of R12-Alexa, analyzed by confocal laser scanning microscopy without fixation (E) and by flow cytometry (F). Scale bars represent 50 μm. Peptide concentration, 10 μM. Data are shown as the mean ± SD of three independent experiments performed on different days. Asterisks indicate statistically significant differences compared to the negative-control cells. ****$p < 0.0001$ (unpaired Student's t test).

(G) Treating the cells with a CXCR4-specific antagonist, FC131, also inhibited the cellular uptake of R12-Alexa. Peptide and transferrin concentrations were 10 μM and 20 μg/ml, respectively. Data are shown as the mean ± SD of three independent experiments performed on different days. Asterisks indicate statistically significant differences compared to the negative-control cells. ****$p < 0.0001$ (two-way ANOVA followed by Bonferroni's post hoc test).

(H) Live cell analysis of the colocalization of R12-Alexa568 with CXCR4-Venus on the cell surface. Cells were treated with 5 μM R12-Alexa568 for 10 min at 4°C and the surfaces of live cells facing the bottom glass were observed by confocal laser scanning microscopy. Scale bars represent 5 μm.

(I) Treatment with the Gi signaling-pathway inhibitor PTX (100 ng/ml) yielded decreased cellular uptake of R12-Alexa but not R8- or Tat-Alexa. Peptide and transferrin concentrations were 10 μM and 50 μg/ml, respectively. Data are shown as the mean ± SD of three or four values obtained from independent experiments performed on different days. Asterisks indicate statistically significant differences from the no-inhibitor groups. ****$p < 0.0001$ (two-way ANOVA followed by Bonferroni's post hoc test).

See also Figure S1.

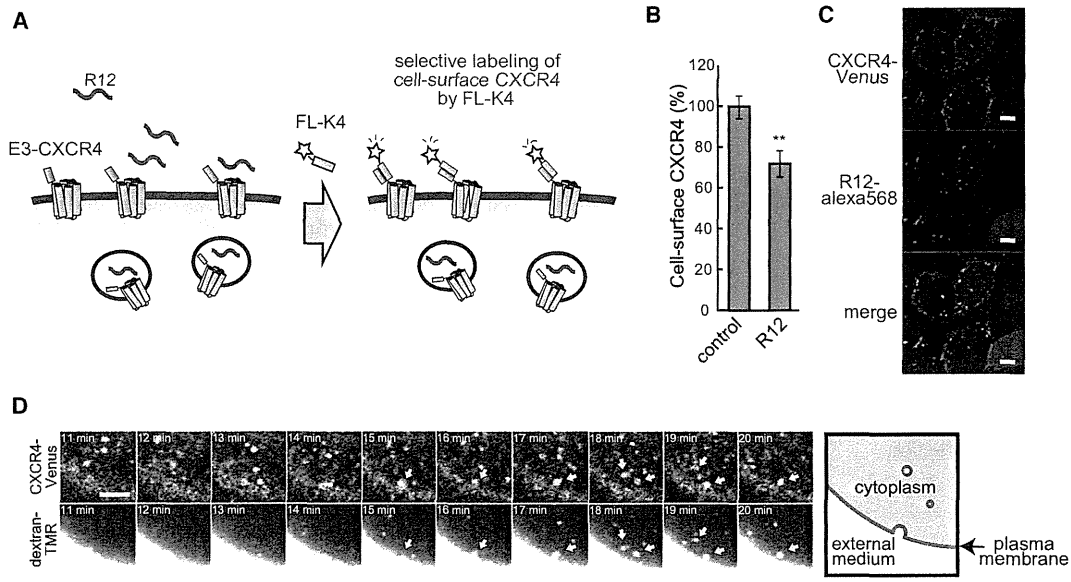

Figure 2. Internalization of CXCR4 by Treatment with R12

(A) Specific labeling of E3-tagged CXCR4 on cell surfaces using fluorescently labeled K4 probe.

(B) Internalization of CXCR4 following R12 treatment. CHO cells expressing E3-CXCR4 were treated with nonlabeled R12 (10 μM) for 30 min, and then the amount of the CXCR4 remaining on the cell surface was analyzed by treatment with E3-specific fluorescein-labeled K4 peptide (FL-K4). Data are shown as the mean ± SD of three independent experiments. Asterisks indicate statistically significant differences from control cells. **$p < 0.01$ (unpaired Student's t test).

(C) Colocalization of R12 with CXCR4 after cell treatment with 5 μM R12-Alexa568 for 30 min at 37°C. The live cells were then analyzed directly by confocal laser scanning microscopy without fixation. Scale bars represent 5 μm.

(D) CXCR4 internalizes into cells with the macropinocytosis marker dextran-TMR (70 kDa). CHO-C4V cells were treated with 10 μM nonlabeled R12 together with dextran-TMR (1 mg/ml) and observed by time-lapse imaging. Significant colocalization of the CXCR4-Venus and dextran-TMR signals was observed, suggesting that they were captured in the same endosomal vesicles. Yellow arrows indicate that the vesicles contain both CXCR4-Venus and dextran-TMR. The scale bar represents 5 μm.

See also Figure S2.

Interestingly, no significant reduction in R8 or Tat (10 μM) cellular uptake was observed in CXCR4-knockdown cells (Figure 1F), and similar patterns were observed in FC131-treated cells (Figure 1G). Thus, CXCR4 was not responsible for the cellular uptake of these peptides. The R8 and Tat peptides are typical arginine-rich CPPs with a smaller number of arginines in their sequences than R12 (Futaki, 2006; Kosuge et al., 2008), suggesting diversity in cellular uptake mechanisms even among arginine-rich peptides.

Cell-surface interaction of CXCR4 with R12 was confirmed by confocal laser scanning microscopy (Figure 1H). We established CHO cells stably expressing CXCR4 (CHO-C4V) in which a fluorescent protein, Venus, was tagged to the CXCR4 C terminus (cytoplasmic side). Cells were treated with Alexa 568-labeled R12 peptide (R12-Alexa568) at 4°C for 10 min, conditions under which endocytosis does not occur. Significant colocalization of the CXCR4 signals with R12 (Figure 1H) suggested specific binding of R12 to CXCR4 on the cell surface, whereas lower levels of colocalized signals were observed when the cells were treated with Alexa 568-labeled R8 and Tat peptides (Figure S1C).

Binding of CXCR4 to its natural ligand, SDF-1α, leads to actin reorganization via the Gi protein-signaling pathway (Möhle et al., 2001). Indeed, a marked lamellipodia (i.e., thin, veil-like extensions at the edge of cells that contain a dynamic array of actin filaments, typically observed for cells treated with oligoarginine CPPs) formation was observed for control cells by treatment with R12 for 20 min; however, no significant alteration in actin structure was observed in CXCR4-knockdown cells (Figure S1D). Cellular uptake of R12-Alexa was suppressed by 30% in the presence of pertussis toxin (PTX), an inhibitor of the Gi protein-signaling pathway (Phillips and Ager, 2002) (Figure 1I). Furthermore, PTX treatment also led to a significant suppression in the formation of lamellipodia by the R12 peptide (data not shown). These results suggest that CXCR4 serves as an R12 receptor to promote actin organization, together with uptake of the R12 peptide. Involvement of the Gi protein-signaling pathway was suggested in the above process. Here again, cellular uptake of R8 and the Tat peptide was not affected by PTX treatment (Figure 1I).

Treating cells with the R12 peptide led to internalization of the CXCR4 receptor. A coiled-coil tag/probe system, developed by Yano et al. (2008), was used to analyze this result. Specifically, CXCR4 bearing a surface-exposed tag sequence E3 $(EIAALEK)_3$ at the N terminus (E3-CXCR4) was expressed on CHO-K1 cells (Figure 2A). After treating the cells with R12 or other CXCR4 ligands, E3-CXCR4 remaining on the plasma membranes was quantified by a fluorescently labeled E3-specific peptide probe, K4 $(KIAALKE)_4$. This system was expected to more accurately assess the quantities of cell surface-exposed receptors,

compared with conventional methods that use receptor-specific antibodies; binding of receptor-specific antibodies may be hampered when their ligands are tightly bound to the receptor. However, the relatively small K4 probe used in this system allowed us to detect CXCR4 without disruption by ligand binding (Yano et al., 2008). Treating the cells with R12 peptide for 30 min resulted in the internalization of cell-surface CXCR4; an ~30% decrease in the amount of CXCR4 on cell surfaces was observed following this treatment compared with nontreated cells (Figure 2B).

The intracellular fate of CXCR4 after binding with R12 was then analyzed using the CXCR4-Venus system employed in Figure 1H, but this time cells were incubated at 37°C to allow endocytic cellular uptake. Treatment of the cells with R12-Alexa for 30 min led to internalization of CXCR4 and significant colocalization of the R12-Alexa568 signal with CXCR4 in the cytoplasm (Figure 2C). On the other hand, large amounts of CXCR4 remained on the cell surface, even after treatment with R8- and Tat-Alexa568, which yielded considerably fewer colocalized signals in the cytoplasm compared to R12 treatment (Figure S2A). Time-lapse imaging of CXCR4-Venus cells treated with a macropinosome marker (70 kDa dextran labeled with tetramethylrhodamine; dextran-TMR) in the presence of R12 peptide showed significant colocalization of the signals of Venus and TMR, indicative of CXCR4 internalization via the macropinocytic pathways stimulated by the R12 peptide (Figure 2D). Because endosomes formed by macropinocytosis (i.e., macropinosomes) can be CXCR4-Venus signals colocalizing with dextran-TMR, compared with those without significant colocalization (see Figure S2B), this also suggests that these signals represent macropinosomes. Thus, CXCR4 serves as a receptor of R12 and is internalized into cells via macropinocytosis together with R12.

Note that the above observation would not necessarily indicate CXCR4-mediated macropinocytosis as the sole and exclusive pathway for R12 uptake. R8 and other arginine-rich peptides also employ macropinocytosis for their cellular uptake (Nakase et al., 2004); as shown in this study, the methods are not identical to that using CXCR4. However, it could be possible that a part of R12 may also be internalized in the cells using similar methods employed by R8. Dynasore is an inhibitor of dynamin that is critically involved in clathrin- or caveolae-mediated endocytosis. Treating the cells with dynasore yielded an ~35% decrease in 5 μM R12 uptake (Figure S2C). This result suggests the possibility that certain dynamin-dependent endocytic pathways may be involved in the cellular uptake of R12 simultaneously with macropinocytosis. Additionally, only an ~10% reduction in the cellular uptake of R8 was observed under the same dynasore treatment (Figure S2C). The relative insensitivity of R8 uptake by dynasore may again suggest differences in the methods of cellular uptake between R12 and R8.

Stimulation of CXCR4 by SDF-1α or HIV-1 gp120 Also Leads to Macropinocytosis

If stimulating CXCR4 with R12 induces actin organization and its macropinocytic uptake, it is possible that stimulating the receptor with other ligands may also stimulate macropinocytosis. SDF-1α is a typical CXCR4 ligand, and the involvement of actin reorganization through CXCR4 activation has been reported (Voermans et al., 2001; Wu and Yoder, 2009). It has been reported that ligand binding to CXCR4 leads to its internalization via clathrin-dependent endocytosis (Signoret et al., 1997; Orsini et al., 1999; Venkatesan et al., 2003). However, there is no report of the relevance of actin reorganization through CXCR4 activation to macropinocytosis induction. In this context, we examined whether stimulation of CXCR4 with SDF-1α may lead to macropinocytosis in addition to actin organization and an eventual increase in its cellular uptake.

Treating HeLa cells with SDF-1α led to an increase in cellular uptake of 70 kDa dextran of ~110%, and the increase in 70 kDa dextran uptake by SDF-1α stimulation was inhibited by 40% in the presence of ethylisopropylamiloride (EIPA), a typical macropinocytosis inhibitor (Nakase et al., 2004) (Figure 3A). SDF-1α also induces actin organization, and significant lamellipodia formation was also observed for SDF-1α-treated cells (Figure 3B). These observations suggest the induction of macropinocytosis following CXCR4 stimulation with its natural ligand SDF-1α. Quantifying the cell-surface receptor using E3-tagged CXCR4, as used in Figure 2B, showed that stimulating CXCR4 with SDF-1α led to a decrease in cell surface-expressed CXCR4 by ~65% (Figure 3C). A confocal microscopic analysis showed that CXCR4 tagged with Venus was internalized into the cells following treatment with SDF-1α (Figure 3D). Colocalization of the CXCR4-Venus signals with those of 70 kDa dextran suggests the localization of CXCR4 in macropinosomes. To the best of our knowledge, this is the first demonstration that stimulating CXCR4 with SDF-1α leads to macropinocytosis and the eventual internalization of CXCR4.

Considerable research has focused on macropinocytosis and its relevance to viral infections (Mercer and Helenius, 2009). We not only identified CXCR4 as a receptor that induces macropinocytosis but also showed that the receptor is internalized in cells and is trapped in macropinosomes bound to its ligand. HIV infection of target cells is accomplished on the cell surface, and CXCR4 serves as a CD4 protein coreceptor to stimulate viral binding and successive fusion to the plasma membranes, allowing entry of the viral nucleocapsid. Thus, if HIV binding to CXCR4 induces macropinocytosis, HIV may become trapped in macropinosomes and delivered to cells.

HIV-1 gp120 is a glycoprotein present on the surface of the viral envelope and is essential for CXCR4 binding, leading to virus entry into cells (Tamamura et al., 2005). Treatment of HeLa cells with 500 nM gp120 induced a 25% increase in 70 kDa dextran uptake in 60 min (Figure 3E). Significant lamellipodia formation was also observed 20 min after administering gp120 (Figure 3B). These results suggest that macropinocytosis may accompany HIV entry into cells (Wu and Yoder, 2009).

Effect of R12 Treatment and Macropinocytosis on HIV Infection of Host Cells

$HIV\text{-}1_{IIIB}$ is a subtype of HIV-1 that uses CXCR4 as a coreceptor for entry into susceptible cells. Anti-HIV infection activity of R12 for $HIV\text{-}1_{IIIB}$ was analyzed using a T cell line, MT-4, which is highly susceptible to HIV infection (Koyanagi et al., 1985). The cells were incubated with $HIV\text{-}1_{IIIB}$ in the presence of R12 or R8 for 5 days and cell viability was analyzed using the MTT (3-[4,5-dimethylthiazol-2-yl]-2,5-diphenyltetrazolium bromide) assay as reported previously (Kodama et al., 2001), yielding a 50%

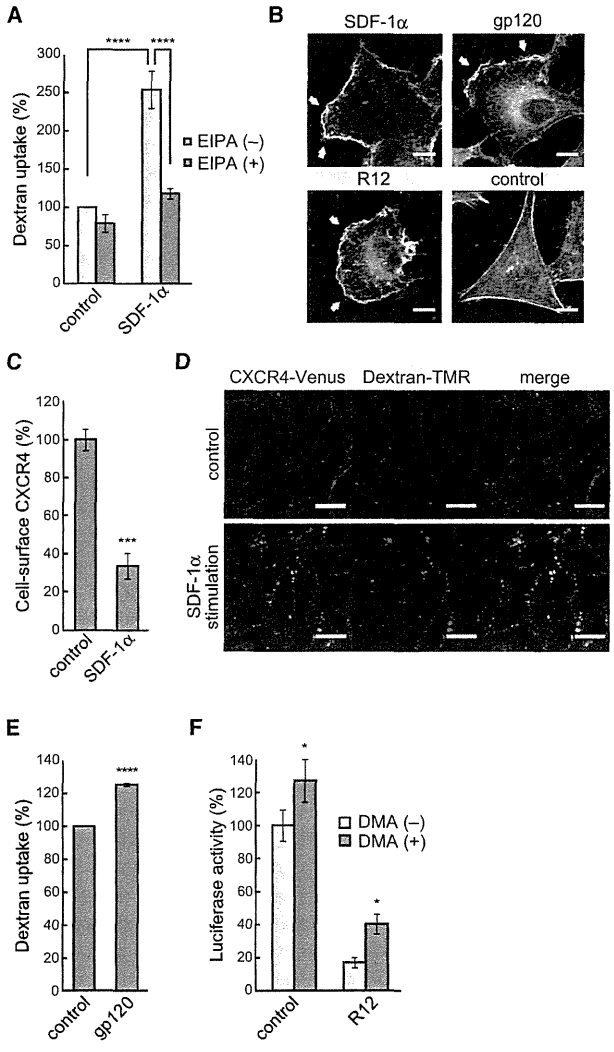

Figure 3. Stimulating CXCR4 with SDF-1α and gp120 Induces Actin Organization and Macropinocytosis

(A) Increase in 70 kDa dextran-fluorescein uptake in HeLa cells following treatment with 100 nM SDF-1α for 1 hr. Pretreatment with EIPA (100 μM) diminished the dextran uptake. Data are shown as the mean ± SD of three independent experiments. Asterisks indicate statistically significant differences from control cells. ****p < 0.0001 (two-way ANOVA followed by Bonferroni's post hoc test).

(B) Actin cytoskeleton rearrangement by SDF-1α and gp120. HeLa cells were treated with SDF-1α (100 nM), gp120 (500 nM), and R12 (10 μM) for 20 min. The cells were fixed with 4% paraformaldehyde, and cellular F-actin was stained with phalloidin-tetramethylrhodamine isothiocyanate. White arrows indicate lamellipodia. Scale bars represent 10 μm.

(C) Internalization of CXCR4 following treatment with 100 nM SDF-1α (30 min). The experiments were conducted using E3-CXCR4 cells and FL-K4 as in Figure 2B. Data are shown as the mean ± SD of three independent experiments. Asterisks indicate statistically significant differences from control cells. ***p < 0.001 (unpaired Student's t test).

(D) Treating CHO-C4V cells with 100 nM SDF-1α led to the internalization of CXCR4-Venus by cells. CXCR4-Venus signals showed high colocalization with the macropinosome marker 70 kDa dextran-TMR. Control cells showed less internalization of CXCR4-Venus and 70 kDa dextran-TMR, yielding little colocalization with 70 kDa dextran-TMR signals. Scale bars represent 10 μm.

(E) HIV-1 envelope protein gp120 (500 nM) induces macropinocytosis. HeLa cells were treated with 500 nM gp120, as shown in (A), for 1 hr. Data are shown as the mean ± SD of three independent experiments. Asterisks indicate statistically significant differences from control cells. ****p < 0.0001 (unpaired Student's t test).

(F) Inhibition of HIV infection in the presence of a macropinocytosis inhibitor. MT-4 cells were pretreated with DMA for 30 min at 37°C. HIV-based luciferase expression vector pseudotyped with HIV-1_{IIIB} envelope was used to infect DMA-treated or untreated cells in the absence or presence of 5 μM R12. After 48 hr of culture, luciferase activity was measured. Data are shown as the mean ± SD of three independent experiments performed in duplicate. Asterisks indicate statistically significant differences from cells treated without inhibitor. *p < 0.05 (unpaired Student's t test).

Table 1. Antiviral Activities against HIV-1_{IIIB} Determined by MTT Assay

Peptide	Mean EC_{50} (nM) ± SD	Mean CC_{50} (nM) ± SD
R12	394 ± 28	>1,000
R8	>1,000	>1,000

Data shown are means and standard deviations obtained from three independent assays.

effective concentration (EC_{50}) of 394 ± 28 nM for the R12 peptide and >1,000 nM for R8 (Table 1). The 50% cytotoxic concentration (CC_{50}) of both peptides was >1,000 nM. The anti-HIV activity of R12 for HIV-1_{IIIB} was also confirmed using a single-round MAGI assay (multinuclear activation of a galactosidase indicator assay; Kimpton and Emerman, 1992) with an EC_{50} value of 332 ± 76 nM (AZT reference, 22 ± 2 nM) (Table 2), whereas no inhibitory effect of R12 (EC_{50} > 10 μM; AZT reference, 23 ± 8 nM) was observed for HIV-1_{BaL} infection using CCR5, instead of CXCR4, as a coreceptor. This suggests that CXCR4 is the target for R12 inhibition or that the internalization of the receptor results in HIV entry inhibition.

Macropinocytosis stimulates internalization of CXCR4 as well as viral uptake into endosomes, which may decrease the chance of HIV entry into host cells via cell-surface fusion (Schaeffer et al., 2001). The effect of macropinocytosis on HIV entry was also assessed using an HIV-1-based firefly luciferase expression vector pseudotyped with HIV-1_{IIIB} envelope. MT-4 cells were treated with dimethylamiloride (DMA), a typical inhibitor of macropinocytosis that has been employed for the analysis of dendritic cell-mediated HIV-1 endocytosis (Maréchal et al., 2001), for 30 min prior to infection and incubated for 48 hr. Treatment of the cells with DMA resulted in an ~30% increase in luciferase activity, suggesting that inhibition of macropinocytosis improves viral infection (Figure 3F, left). There was a significant decrease (~70%) in luciferase activity in the presence of R12, confirming the HIV inhibitory effect of the peptide (Figure 3F, right). However, this effect was diminished by pretreatment with DMA (Figure 3F, right).

DISCUSSION

Scientific interest in arginine-rich CPPs has been increasing due to their ability to bring exogenous molecules into cells. The ability of arginine-rich CPPs to induce macropinocytosis is one explanation for their cellular uptake. Although several membrane proteins have previously been considered as potential

Table 2. Antiviral Activities Determined by MAGI Assay

	Mean EC_{50} (nM) ± SD	
Strain	R12	AZT
HIV-1_{IIIB}	332 ± 76	22 ± 2
HIV-1_{BaL}	>10,000	23 ± 8

Data shown are means and standard deviations obtained from three independent assays. AZT (a nucleoside analog reverse-transcriptase inhibitor) was used as a control.

candidates that activate macropinocytosis, or even other forms of endocytosis, specifically responsible for the cellular uptake of arginine-rich CPPs, no substantive receptor has been identified. It has been reported, for example, that the full-length Tat protein (86 residues) could activate a vascular endothelial growth factor receptor (Mitola et al., 1997), but the basic domain (positions 46–64 of the Tat protein corresponding to the CPP segment) was not a high-affinity ligand for the receptor (Rubio Demirovic et al., 2003). It has also been reported that the full-length Tat protein binds to CXCR4 and works as an antagonist against the infection of HIV (Xiao et al., 2000). Interestingly, the basic segment corresponding to the CPP segment (residues 48–60) was not responsible for the antagonism activity but rather residues 11–50 of the Tat protein containing the cysteine-rich domain. Therefore, it seems likely that the receptors for the full-length Tat protein may not necessarily work for the receptor of the arginine-rich CPPs. We and others have reported that the interaction of the arginine-rich peptides with the membrane-associated proteoglycans, including syndecans, quickly activates the Rac protein and induces actin organization and macropinocytosis (Gerbal-Chaloin et al., 2007; Nakase et al., 2007, 2009; Letoha et al., 2010). Although the interaction of arginine-rich peptides with membrane-associated proteoglycans may lead to their multimerization to induce actin polymerization, more evidence is required to conclude that these proteoglycans are actual receptors that can induce macropinocytosis; as is seen in the case of FGF2 (Ishihara, 1993), proteoglycans often couple with other receptors to activate them. Additionally, it was recently reported that a complex of oligonucleotides with the stearylated TP-10 analog PepFect14 was taken into cells through scavenger receptors (Ezzat et al., 2012). This was an important finding that may potentially be extendable to enhance the biological effects given by the oligonucleotides. However, recognition of the negative charges of the complex by the receptor, not of the peptides, is considered to be the mechanism.

Using synthetic peptides as chemical tools, we have demonstrated that the CXCR4 chemokine receptor acts as a receptor to stimulate cellular uptake of the R12 peptide. Cellular uptake of R12 was inhibited by CXCR4 siRNA knockdown and by FC131, an antagonist of CXCR4. Treating the cells with R12 led to actin organization (lamellipodia formation) and macropinocytosis, but CXCR4 knockdown effectively prevented the formation of lamellipodia. Confocal microscopy revealed significant colocalization of CXCR4 with the R12 peptide on cell surfaces. Binding of R12 to CXCR4 led to their internalization, and significant colocalization of these signals was observed in macropinosomes in the cells. Treatment of the cells with PTX suppressed the cellular uptake of R12, suggesting the use of a Gi signaling pathway for uptake.

To our knowledge, these results are not only the first report of a substantive receptor to stimulate the uptake of arginine-rich CPPs, but are also the first illustration of intracellular traffic of the receptors involved in R12 uptake after ligand activation. Interestingly, R8 and Tat, other typical arginine-rich CPPs, did not significantly activate this CXCR4-mediated uptake pathway. These peptides are also reported to use macropinocytosis for their cellular uptake (Nakase et al., 2004, 2007). R12 has a higher internalization efficiency than the R8 and Tat peptides (Nakase et al., 2007; Kosuge et al., 2008), and the higher valency of the guanidino groups in a peptide to ensure greater interaction with cell-surface molecules has been suggested as one explanation (Futaki, 2006; Wender et al., 2008). However, the present study indicates that the lack of CXCR4-mediated activation of macropinocytosis by R8 and Tat may explain the higher cellular uptake efficiency of R12 over these peptides. In addition, if the cooperation of CXCR4 and syndecan-4 is important for receptor activation, R12 may stabilize these complex structures.

We also found that stimulation of CXCR4 with an intrinsic ligand, SDF-1α, induced macropinocytosis. This study also suggests that macropinocytosis is induced by the interaction of HIV-1 with CXCR4 on host cell membranes, which leads to the internalization of the receptor during viral infection of the host cells. Although the involvement of macropinocytosis with HIV-1 internalization has been observed in specific cells such as dendritic cells (Wang et al., 2008), macropinocytosis operates only for housekeeping in these cells, and there should be distinct differences in the methods of internalization in the many cells where macropinocytosis is induced only by external stimuli. Our study suggests that macropinocytosis stimulates internalization of CXCR4 as well as viral uptake into late endosomes, which may decrease the chance of HIV entry into host cells via cell-surface fusion and promote viral degradation in endosomes (Schaeffer et al., 2001). Thus, macropinocytosis induced by the interaction with HIV-1 may eventually work as a protective response by host cells against a viral invasion. In this context, R12 shows inhibitory activity against HIV-1 infection; interaction of R12 with CXCR4 leads to internalization of the receptor as well as viral uptake via macropinocytosis, both of which may inhibit viral infection. ALX40-4C is an anti-HIV-1 peptide (acetyl-[D-Arg]$_9$-amide) (Doranz et al., 1997; Zhang et al., 2002), having structural similarity with R8 and R12. The anti-HIV-1 activity of ALX40-4C has been claimed to be exclusively by blocking virus-CXCR4 interactions (Doranz et al., 2001), and this would also be one mechanism of the anti-HIV-1 activity of R12. Detailed studies of the effect of ALX40-4C on CXCR4 internalization and macropinocytosis induction would be beneficial to better understand the contribution of macropinocytosis to the inhibition of HIV-1 infection.

SIGNIFICANCE

This report has shed light on the roles of CXCR4 as a receptor for stimulating cellular uptake of arginine-rich cell-penetrating peptides and the induction of macropinocytosis, which should have implications for cellular responses, accompanied by intracellular delivery using oligoarginines, and for HIV infection.

EXPERIMENTAL PROCEDURES

Preparation of Biotin-TmdPhe-R12 and Biotin-TmdPhe-R4

H-GABA-TmdPhe-Gly-(Arg[Pbf])$_{12}$-NH-resin (GABA, γ-aminobutyric acid; Pbf, 2,2,4,6,7-pentamethyldihydrobenzofuran-5-sulfonyl) was prepared by Fmoc (9-fluorenylmethyloxycarbonyl) solid-phase peptide synthesis on a Rink amide resin, as described previously (Kosuge et al., 2008; Nakase et al., 2009), in which the TmdPhe was assembled into the peptide chain using Fmoc-TmdPhe, as is the case with other amino acids. Biotin was then introduced onto the peptide resin using biotinamidohexanoic acid N-hydroxysuccinimide ester (Sigma) to yield biotinamidohexanoyl-GABA-TmdPhe-Gly-(Arg[Pbf])$_{12}$-NH-resin. The peptide was deprotected and cleaved from the resin by treatment with a trifluoroacetic acid/ethanedithiol mixture (95:5), followed by reverse-phase high-performance liquid chromatography purification to yield biotinamidohexanoyl-GABA-TmdPhe-Gly-(Arg)$_{12}$-amide (biotin-TmdPhe-R12). The mass of the product was confirmed by MALDI-TOF MS: 2629.99 (calculated for $[M+H]^+$ 2629.14). Biotin-TmdPhe-R4 was similarly prepared as biotin-TmdPhe-R12. MALDI-TOF MS: 1380.81 (calculated for $[M+H]^+$ 1379.61).

Photocrosslinking

HeLa cells (1.2×10^6) were plated on 100 mm dishes and cultured in α-minimum essential medium (α-MEM) containing 10% heat-inactivated bovine serum (α-MEM/BS) for 48 hr. After the cells were washed three times with PBS(+), they were treated with biotin-TmdPhe-R12 (0.5 μM) or biotin-TmdPhe-R4 (1.5 μM) for 30 s at 37°C and then irradiated with a UV lamp with a 365 nm filter for 3 min at 4°C. Cells were washed with PBS(+) twice and lysed in RIPA buffer (100 μl) containing 150 mM NaCl, 10 mM Tris-HCl (pH 7.2), 0.1% SDS, 1.0% NP-40, 1% deoxycholate, and 5 mM EDTA. Lysates were then dialyzed against 1,000 ml PBS at 4°C for 12 hr using a Slide-A-Lyzer (molecular weight cutoff 20,000; Pierce).

The protein concentration of the above lysates was adjusted to yield 500 μg protein/500 μl RIPA buffer, and 10% SDS (214 μl) in water was added to yield a protein solution containing 3% SDS. Streptavidin magnetic spheres (Promega; 300 μl) were then added to the solution. After gently mixing at 20°C for 1 hr, the streptavidin magnetic spheres, bearing proteins crosslinked with biotin-TmdPhe-R12, were collected with a magnet and washed with RIPA buffer, and then the sample buffer for SDS-PAGE (40 μl) containing 3% SDS and 10% 2-mercaptoethanol was added. After heat denaturation at 85°C for 5 min, the mixtures were subjected to electrophoresis. Prior to PMF analysis, the samples were analyzed by 7.5% SDS-PAGE using silver staining. Protein bands positive in biotin-TmdPhe-R12-treated cells but negative in biotin-TmdPhe-R4-treated cells were collected, trypsinized, and subjected to MALDI-TOF MS/PMF analysis. Western blotting was conducted using 10% SDS-PAGE prior to sample transfer to PVDF membranes. Anti-CXCR4 antibody (1:1,000; ab2074; Abcam), anti-syndecan-4 antibody (1:1,000 dilution; 5G9; Santa Cruz Biotechnology), and anti-CD71 antibody (1:200 dilution; sc-9099; Santa Cruz Biotechnology), together with the corresponding second antibody conjugated to horseradish peroxidase, were used to detect the target proteins.

Confocal Microscopic Observation of CXCR4-Venus and R12-Alexa

CHO-C4V cells (4×10^5 cells/well) stably expressing CXCR4-Venus (see Supplemental Experimental Procedures) were plated on 35 mm glass-bottomed dishes and cultured in an F-12 nutrient mixture containing 10% heat-inactivated fetal bovine serum (F-12/FBS) supplemented with penicillin/streptomycin and hygromycin for 72 hr. After complete adhesion, the cell-culture medium was changed to serum-free F-12 and cells were incubated for 1 hr. The cells were then incubated at 37°C in fresh medium (150 μl) containing 5 μM R12-Alexa568. The cells were washed twice with heparin/PBS, and ice-cold fresh medium without peptides (1 ml) was added. Localization of R12-Alexa568 and CXCR4-Venus in the cells was then analyzed using an FV1000 confocal scanning laser microscope (Olympus) equipped with a 60× objective without fixing the cells. Colocalization with dextran-TMR (70 kDa) was analyzed by incubating CHO-C4V cells with fresh medium containing 10 μM R12 or 100 nM SDF-1α in the presence of 1 mg/ml dextran-TMR for 20 min at 37°C.

To observe CXCR4-Venus and R12-Alexa568 on the cell surface, cells were incubated with serum-free F-12 for 30 min at 4°C and treated with 5 μM R12-Alexa568 for 10 min at 4°C to prevent internalization of CXCR4-Venus. The cells were washed with ice-cold F-12 twice and analyzed with a confocal scanning laser microscope as described above.

Colocalization of R8-Alexa568 and Tat-Alexa568 with CXCR4 was also observed using confocal microscopy similar to that with R12-Alexa568.

CXCR4 Internalization Assay

E3-CXCR4 CHO cells were similarly established as the CHO-C4V cells, and were detached using Versene. Cells (0.4×10^6) were resuspended in F-12 medium containing R12 or SDF-1α (500 μl), incubated at 4°C or 37°C for 30 min, and washed twice with ice-cold PBS containing 0.5% (w/v) heparin and PBS. The cells were treated with 100 nM fluorescein-labeled K4 peptide (FL-K4) (Yano et al., 2008) in F-12 (100 μl) at 4°C for 15 min and analyzed using a FACSCalibur flow cytometer. Ten thousand events were analyzed per sample (n = 3).

SUPPLEMENTAL INFORMATION

Supplemental Information includes three figures and Supplemental Experimental Procedures and can be found with this article online at http://dx.doi.org/10.1016/j.chembiol.2012.09.011.

ACKNOWLEDGMENTS

This work was supported in part by Grants-in-Aid for Scientific Research and the Targeted Protein Research Program from the Ministry of Education, Culture, Sports, Science and Technology of Japan. R.M. is grateful for research fellowships from the Japan Society for the Promotion of Science for Young Scientists. This study was also supported by the Swedish Research Council, the Swedish Foundation for Strategic Research, and the Swedish Governmental Agency for Innovation Systems (project no. MDB09-0015) (to Ü.L. and A.G.), and the Strategic Japanese-Swedish Cooperative Program on "Multidisciplinary BIO" from the Japan Science and Technology Agency and VINNOVA (to S.F.).

Received: July 23, 2012
Revised: August 28, 2012
Accepted: September 3, 2012
Published: November 21, 2012

REFERENCES

Arii, J., Goto, H., Suenaga, T., Oyama, M., Kozuka-Hata, H., Imai, T., Minowa, A., Akashi, H., Arase, H., Kawaoka, Y., and Kawaguchi, Y. (2010). Non-muscle myosin IIA is a functional entry receptor for herpes simplex virus-1. Nature *467*, 859–862.

Conner, S.D., and Schmid, S.L. (2003). Regulated portals of entry into the cell. Nature *422*, 37–44.

Doranz, B.J., Grovit-Ferbas, K., Sharron, M.P., Mao, S.-H., Goetz, M.B., Daar, E.S., Doms, R.W., and O'Brien, W.A. (1997). A small-molecule inhibitor directed against the chemokine receptor CXCR4 prevents its use as an HIV-1 coreceptor. J. Exp. Med. *186*, 1395–1400.

Doranz, B.J., Filion, L.G., Diaz-Mitoma, F., Sitar, D.S., Sahai, J., Baribaud, F., Orsini, M.J., Benovic, J.L., Cameron, W., and Doms, R.W. (2001). Safe use of the CXCR4 inhibitor ALX40-4C in humans. AIDS Res. Hum. Retroviruses *17*, 475–486.

Ezzat, K., Helmfors, H., Tudoran, O., Juks, C., Lindberg, S., Padari, K., El-Andaloussi, S., Pooga, M., and Langel, U. (2012). Scavenger receptor-mediated uptake of cell-penetrating peptide nanocomplexes with oligonucleotides. FASEB J. *26*, 1172–1180.

Falcone, S., Cocucci, E., Podini, P., Kirchhausen, T., Clementi, E., and Meldolesi, J. (2006). Macropinocytosis: regulated coordination of endocytic and exocytic membrane traffic events. J. Cell Sci. *119*, 4758–4769.

Fujii, N., Oishi, S., Hiramatsu, K., Araki, T., Ueda, S., Tamamura, H., Otaka, A., Kusano, S., Terakubo, S., Nakashima, H., et al. (2003). Molecular-size reduction of a potent CXCR4-chemokine antagonist using orthogonal combination

of conformation- and sequence-based libraries. Angew. Chem. Int. Ed. Engl. *42*, 3251–3253.

Futaki, S. (2006). Oligoarginine vectors for intracellular delivery: design and cellular-uptake mechanisms. Biopolymers *84*, 241–249.

Futaki, S., Suzuki, T., Ohashi, W., Yagami, T., Tanaka, S., Ueda, K., and Sugiura, Y. (2001). Arginine-rich peptides. An abundant source of membrane-permeable peptides having potential as carriers for intracellular protein delivery. J. Biol. Chem. *276*, 5836–5840.

Gerbal-Chaloin, S., Gondeau, C., Aldrian-Herrada, G., Heitz, F., Gauthier-Rouvière, C., and Divita, G. (2007). First step of the cell-penetrating peptide mechanism involves Rac1 GTPase-dependent actin-network remodelling. Biol. Cell *99*, 223–238.

Hamon, M., Mbemba, E., Charnaux, N., Slimani, H., Brule, S., Saffar, L., Vassy, R., Prost, C., Lievre, N., Starzec, A., and Gattegno, L. (2004). A syndecan-4/CXCR4 complex expressed on human primary lymphocytes and macrophages and HeLa cell line binds the CXC chemokine stromal cell-derived factor-1 (SDF-1). Glycobiology *14*, 311–323.

Ishihara, M. (1993). Biosynthesis, structure, and biological activity of basic FGF binding domains of heparan sulfate. Trends Glycosci. Glycotechnol. *5*, 343–354.

Kimpton, J., and Emerman, M. (1992). Detection of replication-competent and pseudotyped human immunodeficiency virus with a sensitive cell line on the basis of activation of an integrated β-galactosidase gene. J. Virol. *66*, 2232–2239.

Kodama, E.I., Kohgo, S., Kitano, K., Machida, H., Gatanaga, H., Shigeta, S., Matsuoka, M., Ohrui, H., and Mitsuya, H. (2001). 4′-ethynyl nucleoside analogs: potent inhibitors of multidrug-resistant human immunodeficiency virus variants in vitro. Antimicrob. Agents Chemother. *45*, 1539–1546.

Kosuge, M., Takeuchi, T., Nakase, I., Jones, A.T., and Futaki, S. (2008). Cellular internalization and distribution of arginine-rich peptides as a function of extracellular peptide concentration, serum, and plasma membrane associated proteoglycans. Bioconjug. Chem. *19*, 656–664.

Koyanagi, Y., Harada, S., Takahashi, M., Uchino, F., and Yamamoto, N. (1985). Selective cytotoxicity of AIDS virus infection towards HTLV-I-transformed cell lines. Int. J. Cancer *36*, 445–451.

Letoha, T., Keller-Pintér, A., Kusz, E., Kolozsi, C., Bozsó, Z., Tóth, G., Vizler, C., Oláh, Z., and Szilák, L. (2010). Cell-penetrating peptide exploited syndecans. Biochim. Biophys. Acta *1798*, 2258–2265.

Maréchal, V., Prevost, M.-C., Petit, C., Perret, E., Heard, J.-M., and Schwartz, O. (2001). Human immunodeficiency virus type 1 entry into macrophages mediated by macropinocytosis. J. Virol. *75*, 11166–11177.

Meier, O., Boucke, K., Hammer, S.V., Keller, S., Stidwill, R.P., Hemmi, S., and Greber, U.F. (2002). Adenovirus triggers macropinocytosis and endosomal leakage together with its clathrin-mediated uptake. J. Cell Biol. *158*, 1119–1131.

Mercer, J., and Helenius, A. (2008). Vaccinia virus uses macropinocytosis and apoptotic mimicry to enter host cells. Science *320*, 531–535.

Mercer, J., and Helenius, A. (2009). Virus entry by macropinocytosis. Nat. Cell Biol. *11*, 510–520.

Mitola, S., Sozzani, S., Luini, W., Primo, L., Borsatti, A., Weich, H., and Bussolino, F. (1997). Tat-human immunodeficiency virus-1 induces human monocyte chemotaxis by activation of vascular endothelial growth factor receptor-1. Blood *90*, 1365–1372.

Möhle, R., Bautz, F., Denzlinger, C., and Kanz, L. (2001). Transendothelial migration of hematopoietic progenitor cells. Role of chemotactic factors. Ann. N Y Acad. Sci. *938*, 26–34, discussion 34–35.

Nakase, I., Niwa, M., Takeuchi, T., Sonomura, K., Kawabata, N., Koike, Y., Takehashi, M., Tanaka, S., Ueda, K., Simpson, J.C., et al. (2004). Cellular uptake of arginine-rich peptides: roles for macropinocytosis and actin rearrangement. Mol. Ther. *10*, 1011–1022.

Nakase, I., Tadokoro, A., Kawabata, N., Takeuchi, T., Katoh, H., Hiramoto, K., Negishi, M., Nomizu, M., Sugiura, Y., and Futaki, S. (2007). Interaction of arginine-rich peptides with membrane-associated proteoglycans is crucial for induction of actin organization and macropinocytosis. Biochemistry *46*, 492–501.

Nakase, I., Hirose, H., Tanaka, G., Tadokoro, A., Kobayashi, S., Takeuchi, T., and Futaki, S. (2009). Cell-surface accumulation of flock house virus-derived peptide leads to efficient internalization via macropinocytosis. Mol. Ther. *17*, 1868–1876.

Nakashima, H., Hashimoto, M., Sadakane, Y., Tomohiro, T., and Hatanaka, Y. (2006). Simple and versatile method for tagging phenyldiazirine photophores. J. Am. Chem. Soc. *128*, 15092–15093.

Orsini, M.J., Parent, J.L., Mundell, S.J., Marchese, A., and Benovic, J.L. (1999). Trafficking of the HIV coreceptor CXCR4. Role of arrestins and identification of residues in the C-terminal tail that mediate receptor internalization. J. Biol. Chem. *274*, 31076–31086.

Phillips, R., and Ager, A. (2002). Activation of pertussis toxin-sensitive CXCL12 (SDF-1) receptors mediates transendothelial migration of T lymphocytes across lymph node high endothelial cells. Eur. J. Immunol. *32*, 837–847.

Rey, M., Valenzuela-Fernández, A., Urzainqui, A., Yáñez-Mó, M., Pérez-Martínez, M., Penela, P., Mayor, F., Jr., and Sánchez-Madrid, F. (2007). Myosin IIA is involved in the endocytosis of CXCR4 induced by SDF-1α. J. Cell Sci. *120*, 1126–1133.

Rubio Demirovic, A., Canadi, J., Weiglhofer, W., Scheidegger, P., Jaussi, R., and Kurt, B.-H. (2003). HIV TAT basic peptide is not a high-affinity ligand for VEGF receptor 2. Biol. Chem. *384*, 1435–1441.

Schaeffer, E., Geleziunas, R., and Greene, W.C. (2001). Human immunodeficiency virus type 1 Nef functions at the level of virus entry by enhancing cytoplasmic delivery of virions. J. Virol. *75*, 2993–3000.

Schramm, B., Penn, M.L., Speck, R.F., Chan, S.Y., De Clercq, E., Schols, D., Connor, R.I., and Goldsmith, M.A. (2000). Viral entry through CXCR4 is a pathogenic factor and therapeutic target in human immunodeficiency virus type 1 disease. J. Virol. *74*, 184–192.

Signoret, N., Oldridge, J., Pelchen-Matthews, A., Klasse, P.J., Tran, T., Brass, L.F., Rosenkilde, M.M., Schwartz, T.W., Holmes, W., Dallas, W., et al. (1997). Phorbol esters and SDF-1 induce rapid endocytosis and down modulation of the chemokine receptor CXCR4. J. Cell Biol. *139*, 651–664.

Swanson, J.A., and Watts, C. (1995). Macropinocytosis. Trends Cell Biol. *5*, 424–428.

Tamamura, H., Otaka, A., and Fujii, N. (2005). Development of anti-HIV agents targeting dynamic supramolecular mechanism: entry and fusion inhibitors based on CXCR4/CCR5 antagonists and gp41-C34-remodeling peptides. Curr. HIV Res. *3*, 289–301.

Tkachenko, E., Lutgens, E., Stan, R.-V., and Simons, M. (2004). Fibroblast growth factor 2 endocytosis in endothelial cells proceed via syndecan-4-dependent activation of Rac1 and a Cdc42-dependent macropinocytic pathway. J. Cell Sci. *117*, 3189–3199.

Tomohiro, T., Hashimoto, M., and Hatanaka, Y. (2005). Cross-linking chemistry and biology: development of multifunctional photoaffinity probes. Chem. Rec. *5*, 385–395.

Venkatesan, S., Rose, J.J., Lodge, R., Murphy, P.M., and Foley, J.F. (2003). Distinct mechanisms of agonist-induced endocytosis for human chemokine receptors CCR5 and CXCR4. Mol. Biol. Cell *14*, 3305–3324.

Voermans, C., Anthony, E.C., Mul, E., van der Schoot, E., and Hordijk, P. (2001). SDF-1-induced actin polymerization and migration in human hematopoietic progenitor cells. Exp. Hematol. *29*, 1456–1464.

Wadia, J.S., Stan, R.V., and Dowdy, S.F. (2004). Transducible TAT-HA fusogenic peptide enhances escape of TAT-fusion proteins after lipid raft macropinocytosis. Nat. Med. *10*, 310–315.

Wang, J.-H., Wells, C., and Wu, L. (2008). Macropinocytosis and cytoskeleton contribute to dendritic cell-mediated HIV-1 transmission to $CD4^+$ T cells. Virology *381*, 143–154.

Wender, P.A., Galliher, W.C., Goun, E.A., Jones, L.R., and Pillow, T.H. (2008). The design of guanidinium-rich transporters and their internalization mechanisms. Adv. Drug Deliv. Rev. *60*, 452–472.

Wu, Y., and Yoder, A. (2009). Chemokine coreceptor signaling in HIV-1 infection and pathogenesis. PLoS Pathog. *5*, e1000520.

Xiao, H., Neuveut, C., Tiffany, H.L., Benkirane, M., Rich, E.A., Murphy, P.M., and Jeang, K.T. (2000). Selective CXCR4 antagonism by Tat: implications for in vivo expansion of coreceptor use by HIV-1. Proc. Natl. Acad. Sci. USA *97*, 11466–11471.

Yano, Y., Yano, A., Oishi, S., Sugimoto, Y., Tsujimoto, G., Fujii, N., and Matsuzaki, K. (2008). Coiled-coil tag–probe system for quick labeling of membrane receptors in living cells. ACS Chem. Biol. *3*, 341–345.

Yoder, A., Yu, D., Dong, L., Iyer, S.R., Xu, X., Kelly, J., Liu, J., Wang, W., Vorster, P.J., Agulto, L., et al. (2008). HIV envelope-CXCR4 signaling activates cofilin to overcome cortical actin restriction in resting CD4 T cells. Cell *134*, 782–792.

Zhang, W.-B., Navenot, J.-M., Haribabu, B., Tamamura, H., Hiramatu, K., Omagari, A., Pei, G., Manfredi, J.P., Fujii, N., Broach, J.R., and Peiper, S.C. (2002). A point mutation that confers constitutive activity to CXCR4 reveals that T140 is an inverse agonist and that AMD3100 and ALX40-4C are weak partial agonists. J. Biol. Chem. *277*, 24515–24521.

The International Journal of Biochemistry & Cell Biology 45 (2013) 908–915

Contents lists available at SciVerse ScienceDirect

The International Journal of Biochemistry & Cell Biology

journal homepage: www.elsevier.com/locate/biocel

Mechanism of resistance to S138A substituted enfuvirtide and its application to peptide design

Kazuki Izumi[a], Kumi Kawaji[b], Fusasko Miyamoto[b], Kazuki Shimane[a], Kazuya Shimura[a], Yasuko Sakagami[a], Toshio Hattori[b], Kentaro Watanabe[c], Shinya Oishi[c], Nobutaka Fujii[c], Masao Matsuoka[a], Mitsuo Kaku[d], Stefan G. Sarafianos[e,f], Eiichi N. Kodama[a,b,d,*]

[a] Laboratory of Virus Control, Institute for Virus Research, Kyoto University, 53 Shogoin Kawaramachi, Sakyo-ku, Kyoto 606-8507, Japan
[b] Division of Emerging Infectious Diseases, Tohoku University School of Medicine, Sendai 980-8575, Japan
[c] Department of Bioorganic Medical Chemistry, Division of Physical and Organic Chemistry, Graduate School of Pharmaceutical Sciences, Kyoto University, 46-29 Yoshida Shimoadachi-cho, Sakyo-ku, Kyoto 606-8501, Japan
[d] Division of Infection Control and Laboratory Diagnostics, Tohoku University School of Medicine, Sendai 980-8575, Japan
[e] Christopher S. Bond Life Sciences Center, Department of Molecular Microbiology and Immunology, University of Missouri School of Medicine, Columbia, MO, USA
[f] Department of Biochemistry, University of Missouri School of Medicine, Columbia, MO, USA

ARTICLE INFO

Article history:
Received 31 October 2012
Received in revised form 15 January 2013
Accepted 20 January 2013
Available online 26 January 2013

Keywords:
Resistance
HIV-1
gp41
T-20
Mutation
Fusion inhibitor

ABSTRACT

T-20 (enfuvirtide) resistance is caused by the N43D primary resistance mutation at its presumed binding site at the N-terminal heptad repeat (N-HR) of gp41, accompanied by the S138A secondary mutation at the C-terminal HR of gp41 (C-HR). We have discovered that modifying T-20 to include S138A (T-20_{S138A}) allows it to efficiently block wild-type and T20-resistant viruses, by a mechanism that involves improved binding of T-20_{S138A} to the N-HR that contains the N43D primary mutation. To determine how HIV-1 in turn escapes T-20_{S138A} we used a dose escalation method to select T-20_{S138A}-resistant HIV-1 starting with either wild-type (HIV-1_{WT}) or T-20-resistant (HIV-$1_{N43D/S138A}$) virus. We found that when starting with WT background, I37N and L44M emerged in the N-HR of gp41, and N126K in the C-HR. However, when starting with HIV-$1_{N43D/S138A}$, L33S and I69L emerged in N-HR, and E137K in C-HR. T-20_{S138A}-resistant recombinant HIV-1 showed cross-resistance to other T-20 derivatives, but not to C34 derivatives, suggesting that T-20_{S138A} suppressed HIV-1 replication by a similar mechanism to T-20. Furthermore, E137K enhanced viral replication kinetics and restored binding affinity with N-HR containing N43D, indicating that it acts as a secondary, compensatory mutation. We therefore introduced E137K into T-20_{S138A} (T-$20_{E137K/S138A}$) and revealed that T-$20_{E137K/S138A}$ moderately suppressed replication of T-20_{S138A}-resistant HIV-1. T-$20_{E137K/S138A}$ retained activity to HIV-1 without L33S, which seems to be a key mutation for T-20 derivatives.

Our data demonstrate that secondary mutations can be consistently used for the design of peptide inhibitors that block replication of HIV resistant to fusion inhibitors.

1. Introduction

Human immunodeficiency virus type 1 (HIV-1) fusion to host cell membrane is mediated by formation of a six-helix bundle of the transmembrane subunit gp41 (Chan et al., 1997). Peptides corresponding to amino acid sequences of the gp41 carboxyl-terminal heptad repeat (C-HR) inhibit the HIV-1 fusion by acting as decoys and interfering with the formation of the six-helix bundle (Chan et al., 1998; Malashkevich et al., 1998). Although modified peptides such as SC34EK (Nishikawa et al., 2009), T-2635 (Dwyer et al., 2008), and D-peptides (Welch et al., 2007), and small molecules (Debnath et al., 1999) have been developed, T-20 (enfuvirtide) is the only fusion inhibitor approved for HIV therapy. It is a 36 amino acid peptide derived from the sequence of C-HR of gp41. It is thought to bind at the N-HR domain of gp41 and interfere with the C-HR-N-HR interactions required for membrane fusion and injection of virus into the host cell. T-20 has potent anti-HIV-1 activity and effectively suppresses replication of HIV-1 *in vivo* (Kilby et al., 1998; Lalezari et al., 2003; Lazzarin et al., 2003). However, HIV-1 rapidly develops resistance through mutations in the amino-terminal HR (N-HR) of gp41, especially in the region between L33 and L45, which

* Corresponding author at: Division of Emerging Infectious Diseases, Tohoku University School of Medicine, Sendai 980-8575, Japan. Tel.: +81 22 717 7199; fax: +81 22 717 7199.
E-mail addresses: kodama515@med.tohoku.ac.jp, kodausa21@gmail.com (E.N. Kodama).

1357-2725/$ – see front matter © 2013 Elsevier Ltd. All rights reserved.
http://dx.doi.org/10.1016/j.biocel.2013.01.015

is thought to be the binding site of T-20 (Aquaro et al., 2006; Cardoso et al., 2007; He et al., 2008). Among these residues, N43D in the N-HR is one of the representative mutations for resistance to T-20 (Bai et al., 2008; Cabrera et al., 2006; Oliveira et al., 2009; Izumi et al., 2009; Ueno et al., 2009). Interestingly, most variants show impaired replication fitness, and thus often go on to acquire secondary mutations, such as S138A (Xu et al., 2005), in the C-HR region of gp41 that corresponds to the sequence of T-20. We and others have recently demonstrated that S138A functions as secondary resistance mutation and enhances resistance to T-20 by restoring impaired replication kinetics of T-20-resistant variants that contain primary mutations in the N-HR region, most notably N43D (Izumi et al., 2009; Watabe et al., 2009).

To preempt this escape strategy, we have previously designed a peptide analog of T-20 with the S138A change incorporated in it (T-20_{S138A}; Fig. 1A) and showed that this peptide significantly suppresses replication of T-20-resistant HIV-1 through enhancement of binding affinity to mutated N-HR, such as N-HR_{N43D} (Izumi et al., 2009). Using circular dichroism (CD) and structural analyses, we also demonstrated that the S138A change provided increased stability to the six-helix bundle (Watabe et al., 2009). In subsequent studies, we validated our approach on another peptide-based fusion inhibitor, C34. In this case, we designed a variant of C34 carrying a secondary escape mutation, N126K, selected for the induction of C34 resistance (Nameki et al., 2005) and also present in HIV-1 isolates from T-20 experienced patients (Baldwin et al., 2004; Cabrera et al., 2006; Svicher et al., 2008). We showed that this C34 variant can effectively inhibit replication of C34-resistant HIV-1. These studies provided the proof of principle that it is possible to design improved peptide-based fusion inhibitors that are efficient against a major mechanism of drug resistance through introduction of resistance-associated mutation(s).

It remains unknown to this date how HIV-1 develops further resistance to T-20_{S138A}. Moreover, it is not known whether we can expand our strategy and modify T-20_{S138A} to include the secondary mutation(s) that emerge during the selection of T-20_{S138A}-resistant HIV, resulting in a strategy that is applicable to the design of peptides customized to address viral resistance mutations. Hence, in the current study we selected T-20_{S138A}-resistant HIV-1 *in vitro* by a dose-escalating method. We revealed that the resistance mutations that emerged during selection experiments with wild-type or T-20-resistant HIV-1 are located in both the N-HR and the C-HR regions. Furthermore, the I37N and L33S mutations appeared to act as primary mutations for wild-type and T-20-resistant HIV-1, respectively. E137K, a C-HR mutation located in the T-20 sequence, improved replication kinetics and enhanced affinity to N-HR, indicating that E137K acts as a secondary mutation. Introducing the E137K change into the T-20_{S138A} (T-$20_{E137K/S138A}$) resulted into a peptide inhibitor effective against T-20_{S138A}-resistant variants, suggesting that secondary or compensatory mutations can be widely applicable to the design of next generation peptide-based inhibitors that are active against HIV-1 resistant to earlier generation fusion-targeting drugs.

2. Materials and methods

2.1. Cells and viruses

MT-2 and 293T cells were grown in RPMI 1640 medium and Dulbecco's modified Eagle medium-based culture medium, respectively. HeLa-CD4-LTR-β-gal cells were kindly provided by Dr. M. Emerman through the AIDS Research and Reference Reagent Program, Division of AIDS, National Institute of Allergy and Infectious Disease (Bethesda, MD), and used for the drug susceptibility assay, as previously described (Nameki et al., 2005; Nishikawa et al., 2009). Recombinant infectious HIV-1 clones carrying various mutations were generated through site-directed mutagenesis of the pNL4-3 plasmid, as previously described (Nameki et al., 2005; Nishikawa et al., 2009). Each molecular clone was transfected into 293T cells with *Trans*IT (Madison, WI). After 48 h, the supernatants were harvested and stored at −80 °C.

2.2. Antiviral agents

The peptides used in this study (Fig. 1A) were chemically synthesized using standard Fmoc-based solid-phase techniques, as previously described (Oishi et al., 2008; Otaka et al., 2002). An HIV-1 reverse transcriptase inhibitor, 2′,3′-dideoxycytidine (ddC) was purchased from Sigma–Aldrich Japan (Tokyo, Japan) and used as a control.

2.3. Determination of drug susceptibility

Peptide sensitivity of infectious clones was determined by the multinuclear activation of galactosidase indicator (MAGI) assay as previously described (Nameki et al., 2005; Nishikawa et al., 2009). Briefly, the target cells (HeLa-CD4-LTR-β-gal; 10^4 cells/well) were plated in flat 96-well microtiter culture plates. On the following day, the cells were inoculated with the HIV-1 clones (60 MAGI units/well, resulting into 60 blue cells after 48 h incubation) and cultured in the presence of various concentrations of drugs in fresh medium. Forty-eight hours after virus exposure, all the blue cells stained with X-gal (5-bromo-4-chloro-3-indolyl-β-D-galactopyranoside) were counted in each well. The activity of test compounds was determined as the concentration that reduced HIV-1 infection by 50% (50% effective concentration [EC_{50}]).

2.4. Induction of HIV-1 variants resistant to T-20_{S138A}

MT-2 cells were exposed to HIV-1 and cultured in the presence of T-20_{S138A}. Cultures were incubated at 37 °C until an extensive cytopathic effect (CPE) was observed. The culture supernatants were used for further passages in MT-2 cells in the presence of two-fold increasing concentrations of T-20_{S138A} when massive CPEs were seen in the earlier periods. Each passage usually took 5–7 days. The timing is highly dependent on the type of specific mutations introduced, as previously reported (Nameki et al., 2005; Shimura et al., 2010). For example, a passage that follows introduction of novel mutation(s) should shorten the passage period to perhaps 4–5 days. However, there will be longer delays for passages where there are no novel mutations or when there is appearance of only secondary mutations. The dose-escalation process was repeated until resistant variants were obtained. This selection was carried out for a total of 60 passages (approximately 1 year). At the indicated passages (Fig. 1B and C), the sequence of the *env* region was determined by direct sequencing of the proviral DNA extracted from the infected MT-2 cells.

2.5. Viral replication kinetics assay

MT-2 cells (10^5 cells/1 mL) were infected with each virus preparation (500 MAGI units) for 16 h. Infected cells were then washed and cultured in a final volume of 3 mL. The culture supernatants were collected on day 2 through day 5 post-infection, and amounts of p24 antigen were determined.

2.6. CD spectroscopy

Each peptide was incubated at 37 °C for 30 min (the final concentrations of peptides were 10 μM in phosphate buffered saline [PBS];

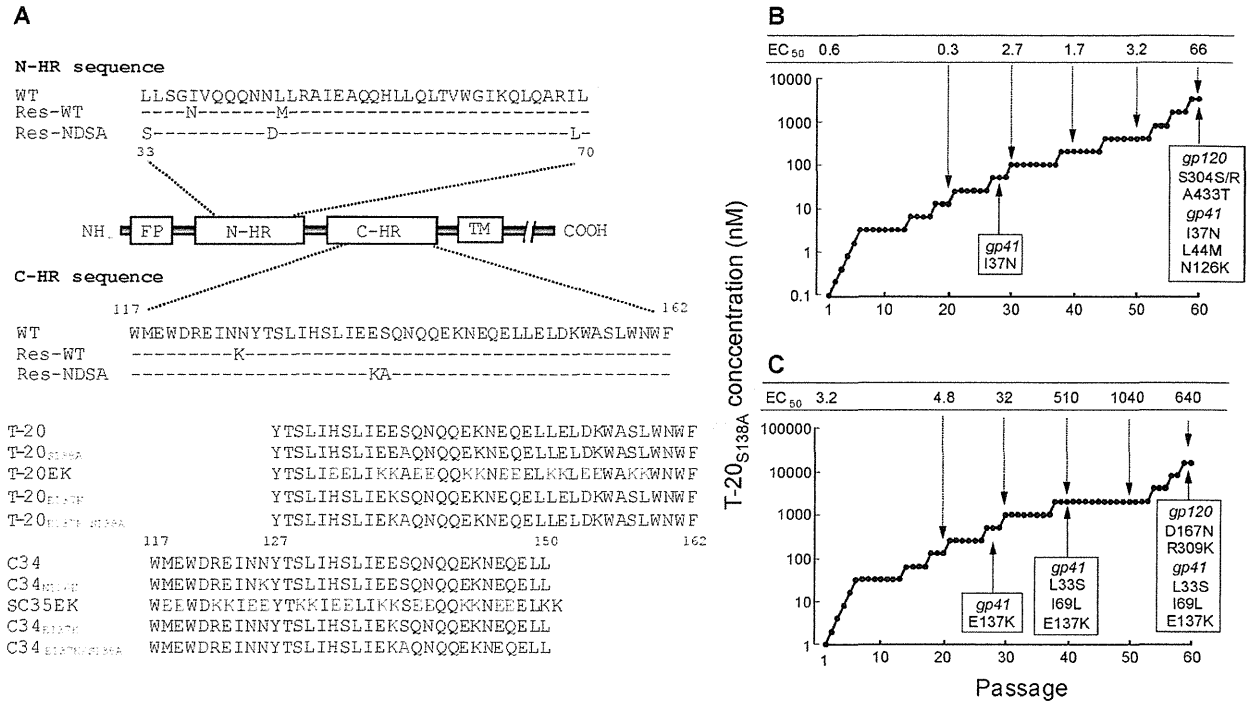

Fig. 1. Domains of gp41 and induction of T-20_{S138A}-resistant HIV-1. (A) Domains of gp41, substitutions observed during *in vitro* passage with T-20_{S138A}, and amino acid sequences of T-20- and C34-based peptides used in this study. The locations of the fusion peptide (FP), amino-terminal heptad region (N-HR), carboxyl-terminal heptad region (C-HR), transmembrane domain (TM), and C-HR-derived peptides are shown. The residue numbers of T-20 and C34 correspond to their positions in gp41. Substitutions of N- and C-HR in gp41 of wild-type (WT) and T-20_{S138A}-resistant HIV-1 are shown. Res.-WT and Res.-NDSA indicate resistant HIV-1 that were initially selected from wild-type and HIV-$1_{N43D/S138A}$, respectively. (B and C) Induction of T-20_{S138A}-resistant HIV-1 by dose-escalating selection in MT-2 cells. Induction of resistant HIV-1 was carried out for a total of 60 passages of HIV-1_{WT} (B) and HIV-$1_{N43D/S138A}$ (C), in 0.1 nM and 1 nM of T-20_{S138A}, respectively. At the indicated passages, proviral DNA was sequenced, and the EC_{50} values of the HIV-1 variants were determined using the MAGI assay. To improve the replication kinetics, substitution of D36G was introduced into the NL4-3 background used in this study (wild-type virus) (Izumi et al., 2009; Mink et al., 2005).

pH 7.4). CD spectra were recorded on an AVIV model 202 spectropolarimeter (Aviv Instruments, Proterion Corporation, Piscataway, NJ) with a 1 mm path-length cuvette at 25 °C as the average of eight scans. The thermal stability was assessed by monitoring the change in the CD signal at 222 nm. The midpoint of the thermal unfolding transition (melting temperature [T_m]) of each complex was determined as previously described (Izumi et al., 2009).

3. Results

3.1. Selection of HIV-1 resistant to T-20_{S138A}

An HIV-1_{NL4-3} strain containing a D36G substitution, which improves replication kinetics, was used as a wild-type virus (HIV-1_{WT}) and for the construction of various mutants, as described (Izumi et al., 2009; Mink et al., 2005). HIV-1_{WT} or T-20-resistant HIV-$1_{N43D/S138A}$ were used for selection of T-20_{S138A}-resistant HIV-1. MT-2 cells were infected with HIV-1_{WT} and HIV-$1_{N43D/S138A}$, and incubated in the presence of T-20_{S138A} at the initial concentrations of 0.1 nM and 1 nM, respectively. At the indicated passages, the sequence of the *env* region was determined by direct sequencing of the proviral DNA extracted from the infected MT-2 cells. During the selection, mutations in the gp41 were observed and are shown in Fig. 1B and C.

In the selection with HIV-1_{WT} (Fig. 1B), at passage 28 (P-28), when T-20_{S138A} concentration was 51.2 nM (P-28, 51.2 nM), isoleucine at position 37 in the gp41 was substituted to asparagine (I37N). At P-60 (3.3 μM), L44 M and N126K in the gp41 further emerged. On the other hand, in the selection with T-20-resistant HIV-$1_{N43D/S138A}$ (Fig. 1C), at P-28 (512 nM) and at P-40 (2 μM), E137K in the gp41, and L33S and I69L in the gp41 emerged, respectively. The emergence of the I69L mutation in diverse HIV-1 strains has been previously reported (Eshleman et al., 2007). At P-60, the resistance of selected viruses from HIV-1_{WT} and HIV-$1_{N43D/S138A}$ to T-20_{S138A}, reached approximately 110- and 200-fold, respectively. These results indicate that even though T-20_{S138A} was active against T-20 resistant variants, resistant HIV-1 emerged relatively rapidly compared with the next generation fusion inhibitors, such as SC34EK, which required 120 passages to acquire the resistance (Shimura et al., 2010).

3.2. Susceptibility of T-20_{S138A}-resistant HIV-1 to T-20 and C34 derivatives

To validate our resistance data we used site-directed mutagenesis to prepare recombinant HIV-1 with the T-20_{S138A}-resistance mutations and examined its susceptibility to T-20 and C34 derivatives with MAGI assay (Table 1). We also used as controls the modified α-helix T-20- and C34-peptide inhibitors, T-20EK (Oishi et al., 2008) and SC35EK (Nishikawa et al., 2009; Shimura et al., 2010), respectively, which are more efficient *in vitro* replication inhibitors of T-20-resistant HIV-1 than T-20 or C34. Finally, we also used as a control $C34_{N126K}$, a modified version of C34 that includes the resistance-associated N126K substitution that effectively suppress replication of C34-resistant HIV-1 *in vitro* (Izumi et al., 2009).

Selected mutations I37N and L33S provided various levels of resistance to T-20 and its derivatives, T-20_{S138A} and T-20EK, apparently acting as primary mutations to peptides with a T-20 backbone (Table 1). Other mutations, L44M, I69L, and E137K, which were